Astron. Astrophys. 295, 75–100 (1995)

ASTRONOMY AND ASTROPHYSICS

Properties of the WO Wolf–Rayet stars

R.L. Kingsburgh [1,2], **M.J. Barlow**[1], **and P.J. Storey**[1]

[1] Department of Physics and Astronomy, University College London, Gower Street, London WC1E 6BT, UK
[2] Instituto de Astronomía, Universidad Nacional Autónoma México, P.O. Box 439027, San Diego, CA 92143-9027, USA

Received 28 February 1994 / Accepted 5 July 1994

Abstract. We present optical spectrophotometry for five WO Wolf–Rayet stars, three of them in our own Galaxy and one in each of the SMC and LMC. *IUE* ultraviolet spectrophotometry has also been obtained for the two Magellanic Cloud WO stars, including a high resolution spectrum for one of them. Quantitative spectral typing criteria are defined for WO subtypes spanning WO1 to WO5 and, for the case of the two WO stars in spectroscopic binaries, spectral types for the O-type primaries are derived. From our spectrophotometry we derive reddenings and magnitudes for each star. Absolute visual magnitudes of -2.5 and -1.8 are derived for a WO4 star and for a WO2 star, respectively, each star lying at a known distance. Wind terminal velocities ranging from 4200 km s^{-1} to 5500 km s^{-1} are derived from the black absorption edge of an ultraviolet P Cygni profile and from the FWZI of strong optical emission lines. The relative abundances of helium, carbon and oxygen in the winds of each of the WO stars are derived using a recombination theory analysis of selected ultraviolet and optical emission lines to determine the ionic abundances of He^{2+}, C^{4+}, O^{4+}, O^{5+} and O^{6+}. The derived abundance ratios show relatively narrow ranges. C/He number ratios of 0.51–0.52 are derived for two Galactic WO stars and one LMC WO star, with their C/O ratios ranging between 4.6 and 5.2, and their (C+O)/He ratios equal to 0.62. The one SMC WO star has a C/He ratio of 0.81, a C/O ratio of 2.7 and a (C+O)/He number ratio of 1.10. These abundance ratios are broadly consistent with evolutionary models for the advanced stages of massive stars, and promising agreement as a function of initial metallicity is found with the most recent evolutionary models.

Key words: stars: Wolf–Rayet – stars: mass-loss – stars: abundances – stars: evolution

1. Introduction

The WO stars are a rare group of highly evolved Wolf–Rayet stars whose spectra are dominated by emission lines from high ionization stages of oxygen and carbon. Wolf–Rayet (WR) stars are believed to be the descendents of massive O-type stars that are presently undergoing extreme mass loss via strong stellar winds – this mass loss has stripped away the outer layers of the stars, revealing the products of nucleosynthesis. The spectra of all WR stars show helium emission lines. Depending on their evolutionary stage, WR spectra are usually dominated by emission lines of nitrogen, carbon or oxygen, and are accordingly classified as WN, WC or WO.

The basis of the present classification scheme for WR stars was laid by Beals & Plaskett (1935), who introduced the WN5–WN8 and WC5–WC8 subtypes. The modern classification scheme for WN and WC stars was introduced by Smith (1968) and was subsequently extended by van der Hucht et al. (1981). The case to physically distinguish the strong oxygen line Wolf–Rayet stars from the WC stars was made by Barlow & Hummer (1982), who introduced the WO classification scheme. They examined the spectra of five stars listed by Sanduleak (1971) as showing strong O VI 3811,34 Å doublet emission. Other strong optical emission lines in the spectra of these stars include the C IV +He II 4658,86 Å blend and the C IV 5801,12 Å doublet, features which are also exhibited strongly by early-WC stars. The WO sequence is defined by the relative strengths of lines due to O IV, O V, O VI and C IV. The original WO sequence of Barlow & Hummer ran from extremely high excitation (WO1) to lower excitation (WO4), where it joined on to the existing WC4 class. In this paper, we extend the WO classification scheme to WO5 and present quantitative classification criteria for the WO class as a whole.

The WO stars were interpreted by Barlow & Hummer (1982) as having evolved past the WC stage, being presently in the late core helium-burning or possibly the carbon-burning stage. The very high degree of ionization of oxygen in their spectra indicates that WO stars are hotter than other Wolf–Rayet stars. The great strength of these oxygen lines was interpreted by Barlow & Hummer as indicating a physical enhancement of the oxygen abundance compared to earlier WR stages, whereby the products of α-particle capture by carbon nuclei during the middle to late stages of core helium burning had been revealed due to mass loss stripping.

We present here an ultraviolet and optical spectroscopic analysis of the original four stars classified as Population I WO

Send offprint requests to: M.J. Barlow

stars by Barlow & Hummer, namely Sand 1 (≡ Sk 188, AB 8), Sand 2 (≡ FD 73, Br 93), Sand 4 (≡ WR 102) and Sand 5 (≡ St 3, WR 142)[1]. Along with their reddenings and terminal velocities, we derive relative helium, carbon and oxygen abundances for these objects. Sand 1 is a WO4 + O7 star, the most luminous member of the young open cluster NGC 602c in the SMC. Sand 2 is a WO4 star in the LMC. Sand 4 is a galactic WO1 star in the nebula G2.4+1.4. Sand 5 is a galactic WO2 star located in the open duster Be 87. Additionally, in this paper we present the WO spectral classification and equivalent widths of the strongest lines for the galactic WO star MS 4 (≡ WR30a, originally named WR29a in the van der Hucht (1981) catalogue). The WO component of MS 4 has been classified as WO4 by Smith et al. (1990a), however we will argue that the WO classification scheme should be extended to WO5, and the WO component of MS 4 placed in this class.

A sixth member of the WO class is DR 1, which is located in the Local Group dwarf irregular galaxy IC 1613, and is surrounded by an H II region[2] with unusually strong nebular He II 4686 in emission. D'Odorico & Rosa (1982) first noted that the WR star in this H II region had peculiar characteristics, remarking on the strength and width of the λλ4658, 4686 and, λλ5801, 5812 features. They classified this star as WCpec or WC+WN. Davidson & Kinman (1982) subsequently analyzed the star and surrounding H II region, and were the first to suggest that it could be a member of the WO class, as they observed O VI 3811,34 Å emission in the stellar spectrum. We have obtained WHT service spectra of DR 1 and its surrounding H II region. Using the classification criteria defined in Sect. 3 of the current paper, the equivalent widths of the strongest stellar emission lines in its spectrum yield a WO3 classification for DR 1 (Sect. 3, and Kingsburgh & Barlow 1995).

2. Observations and data analysis

2.1. IUE observations

Ten low resolution spectra of Sand 1 and three low resolution spectra of Sand 2 have been taken with the *IUE* SWP and LWR cameras. These spectra were accessed via the IUE Uniform Low-Dispersion Archive (ULDA, Talavera 1988). In order to compensate for the decline in sensitivity of the IUE cameras with time, the correction factors of Bohlin & Grillmair (1988) and Clavel et al. (1986) were applied to the SWP and LWR spectra respectively.

Additionally, one 400 minute exposure of Sand 1 has been obtained in high resolution mode with the SWP camera (SWP 7623). This was placed on an absolute scale using the flux calibrated low resolution SWP spectra. In order to derive the appropriate calibration curve, the high resolution spectrum was degraded in resolution to match the low resolution spectra and divided into the weighted average of all the low resolution spectra. A polynomial was fitted to this result and the original high resolution spectrum was multiplied by this polynomial in order to produce a flux calibrated spectrum. Details of the UV observations are presented in Table 1.

Table 1. IUE observations of Sand 1 and Sand 2

	Date	IUE Image No.	Exp. time (min)
Sand 1	Jan. 10 1980	SWP7623H	400
	Aug. 15 1979	SWP6193L	19
	Aug. 15 1979	SWP6194L	6
	Nov. 09 1986	SWP29634L	20
	Nov. 14 1986	SWP29672L	16
	Nov. 17 1986	SWP29700L	16
	Nov. 18 1986	SWP29706L	16
	Nov. 23 1986	SWP29737L	16
	Nov. 24 1986	SWP29744L	16
	Aug. 15 1979	LWR5357L	10
	Jan. 10 1980	LWR6606L	10
Sand 2	Jan. 06 1980	SWP7580L	20
	Jan. 06 1980	SWP7581L	60
	Jan. 06 1980	LWR6556L	60

2.2. Optical observations

Optical spectra of Sand 1, Sand 2, Sand 4 and Sand 5 were acquired with the 3.9-m AAT, using the RGO Spectrograph with the IPCS as detector. A variety of gratings were employed, yielding high to low resolutions. Narrow slit observations (for maximum resolution) and wide slit observations (for absolute spectrophotometry) were made in the 3150–7400 Å region. Higher resolution blue spectra were also obtained for Sand 1 and Sand 4. Additional spectra were obtained at the AAT using the Boller & Chivens Spectrograph with the Image Dissector Scanner (IDS) as detector. Table 2 lists the date, wavelength coverage, resolution, slit width, exposure time and detector for each observation. The AAT IPCS spectral images were reduced using the SDRSYS package (Straede 1980). They were first divided by a normalized flat field. The spatial increments containing the sky background were summed and weighted and subtracted from the central increments containing the object spectrum. Wavelength calibration was performed by means of a fifth order polynomial fit to typically 40 Cu-Ar comparison arc lines. Absolute flux calibration was obtained by means of wide slit observations of white dwarf stars from the list of Oke (1974). In some cases, shorter exposures with neutral density filtering were acquired, in order to obtain unsaturated spectra of the strongest emission

[1] The other star in Sanduleak's (1971) list, Sand 3 (≡ WR 72), is a low mass object (i.e. a planetary nebula central star) – its spectrum was discussed by Barlow et al. (1980) and by Barlow & Hummer (1982).

[2] No. 3 as listed by Sandage (1971)

Table 2. Optical observations

	U.T. Date	Tel.	Det.	Å pix^{-1}	λ coverage (Å)	Sl. Wid. (arcsec)	ND (dex)	Exp. T. (sec)
Sand 1	26 08 78	AAT	IPCS	2.15	3150–7400	0.9	0.88	200
	26 08 78	AAT	IPCS	2.15	3150–7400	6.5	1.46	695
	10 08 78	AAT	IPCS	0.33	3500–4160	1.0	–	600
	06 07 79	AAT	IPCS	0.53	4000–5000	1.5	0.34	900
	06 07 79	AAT	IPCS	0.53	3060–4030	1.0	–	870
	08 07 79	AAT	IPCS	0.27	3750–4240	1.7	–	1300
	04 07 79	AAT	IDS	1.00	5000–6800	2.0	–	120
	22 07 81	AAT	IPCS	0.27	4250–4720	1.5	–	1720
Sand 2	25 04 78	AAT	IDS	1.00	3400–5150	2.0	–	460
	09 10 78	AAT	IPCS	2.15	3150–7400	6.7	–	700
	09 10 78	AAT	IPCS	2.15	3150–7400	6.7	0.88	400
Sand 4	19 04 78	AAT	IPCS	0.50	3680–4630	1.0	–	400
	09 10 78	AAT	IPCS	2.15	3150–7400	6.7	0.34	600
	09 10 78	AAT	IPCS	2.15	3150–7400	6.7	0.88	200
	08 07 79	AAT	IPCS	0.27	3740–4240	1.7	–	604
	04 07 79	AAT	IDS	1.00	3750–5480	2.0	–	360
	13 08 90	JKT	CCD	3.33	7510–9420	1.5	–	1800
Sand 5	26 08 78	AAT	IPCS	2.15	3150–7400	0.9	–	800
	26 08 78	AAT	IPCS	2.15	3150–7400	10.0	0.34	300
	26 08 78	AAT	IPCS	2.15	3150–7400	10.0	1.2	100
	13 08 90	JKT	CCD	3.33	6100–8000	1.5	–	2000
MS 4	18 05 91	AAT	IPCS	0.5	3130–4190	0.4	0.34	1000
	18 05 91	AAT	IPCS	0.5	3130–4190	6.2	0.70	300
	18 05 91	AAT	IPCS	0.5	4040–5090	0.4	0.70	1000
	18 05 91	AAT	IPCS	0.5	4040–5090	6.2	0.70	300
	18 05 91	AAT	IPCS	0.5	4940–6000	0.9	0.70	1000
	18 05 91	AAT	IPCS	0.5	4940–6000	6.2	1.0	300

lines. These spectra were later merged with the deeper spectra, after omitting saturated spectral regions from the latter.

Additionally, red spectra of Sand 4 and Sand 5 have been obtained with a 300 g mm^{-1} grating in the RBS Spectrograph with a UV-coated GEC 590 × 385 pixel CCD as detector, on the 1.0 m JKT at La Palma. Details of these observations are also given in Table 2. These spectra were reduced in a similar manner to that described above, using the STARLINK FIGARO package (Shortridge 1989).

AAT service observations of MS 4 were provided using the RGO Spectrograph with a 1200 g mm^{-1} grating, with the IPCS as detector. Wide and narrow slit spectra were reduced following the procedure described above, also using the FIGARO package. Details of the observations of 5 MS 4 are included in Table 2. The 4.2 m WHT service observations of DR 1 were obtained with the ISIS dual-beam spectrograph, with a CCD detector. Full details are given by Kingsburgh & Barlow (1995).

2.3. *Ultraviolet and optical line fluxes*

All fluxes and equivalent widths (EW's) were measured with the DIPSO package (Howarth & Murray 1988) at the UCL STARLINK node. Table 3 presents the observed ultraviolet emission line EWs and fluxes (F) for Sand 1 and Sand 2, while Table 4 presents the observed optical emission line EW's and fluxes for

Table 3. Ultraviolet equivalent widths, observed (F) and dereddened (I) line fluxes and fractional line contributions, for Sand 1 and Sand 2

			Sand 1				Sand 2			
λ_{obs} (Å)	λ_{id} (Å)	Transition ID's	frac	EW (Å)	F (ergs cm^{-2} s^{-1})	I (ergs cm^{-2} s^{-1})	frac	EW (Å)	F (ergs cm^{-2} s^{-1})	I (ergs cm^{-2} s^{-1})
1343	1342	O IV ($2p^3\ ^2D^0$–$2p^2\ ^2P$)	1.0	6.73±0.04	8.16×10^{-12}	1.10×10^{-11}	1.0	18.3±4.5	4.04×10^{-13}	2.31×10^{-12}
1374	1371	O V ($2p^2\ ^1D$–$2s2p\ ^1P^0$)	1.0	12.68±0.04	1.36×10^{-11}	2.26×10^{-11}	1.0	46.8±5.5	9.77×10^{-13}	5.34×10^{-12}
1403	1402	O IV ($2p^2\ ^4P$–$2p\ ^2P^0$)		–	–	–	1.0	16.9±4.9	3.52×10^{-13}	1.85×10^{-12}
1550	1548,50	C IV ($2p\ ^2P^0$–$2s\ ^2S$)	1.0	56.20±2.26	5.05×10^{-11}	7.97×10^{-12}	1.0	364±14	6.12×10^{-11}	2.78×10^{-11}
1640	1640	He II (3–2)	0.73	9.90±1.18	7.13×10^{-12}	8.77×10^{-12}	0.86	79.7±5.2	1.37×10^{-12}	5.07×10^{-12}
	1640	C IV (6–4)	0.27			3.19×10^{-12}	0.14			7.96×10^{-13}
2080	2070	O VI (6–5)	0.68	6±2	1.8×10^{-12}::	3.98×10^{-12}::		–	–	–
	2082	O VI (8–6)	0.24							
	2084	O VI (11–7)	0.04							
2525	2511	C IV (14–6)	0.02	22±3	4.98×10^{-12}	1.07×10^{-13}	0.02	60.7±5.9	8.06×10^{-13}	4.45×10^{-14}
	2511	He II (7–3)	0.03			1.93×10^{-13}	0.05			1.30×10^{-13}
	2530	C IV (5–4)	0.95			5.94×10^{-12}	0.93			2.39×10^{-12}
2786	2786	O V ($3p\ ^3P^0$–$3s\ ^3S$)	1.0	18.5±1.3	4.21×10^{-12}	4.85×10^{-12}	1.0	43.4±6.6	4.64×10^{-13}	1.27×10^{-12}
2820	2819	C IV (7d–5p) +??	1.0	20.4±2.1	7.06×10^{-13}	7.25×10^{-13}				
2907	2906	C IV (7–5)	0.66	5±2	1.25×10^{-12}::	1.25×10^{-12}::	0.94	25.6±3.1	2.38×10^{-13}	5.85×10^{-13}
	2915	O VI (12–8)	0.34			6.39×10^{-13}::	0.06			3.58×10^{-14}

Table 4. Optical equivalent widths, observed (F) and dereddened (I) line fluxes and fractional line contributions, for Sand 1 and Sand 2

			Sand 1				Sand 2			
λ_{obs} (Å)	λ_{id} (Å)	Transition ID's	frac	EW (Å)	F (ergs cm^{-2} s^{-1})	I (ergs cm^{-2} s^{-1})	frac	EW (Å)	F (ergs cm^{-2} s^{-1})	I (ergs cm^{-2} s^{-1})
3400	3400	O IV (3d ^{2}D–3p ^{2}P^0)[a]	0.91	68.8±1.08	7.33×10^{-12}	8.46×10^{-12}	1.0	299±3	1.40×10^{-12}	3.20×10^{-12}
	3434,38	O VI (7–6, 11–8)	0.09			7.73×10^{-13}				
3700	3690	C IV (9–6,15–7,14–7)		–	–	–	0.24	114±2	3.59×10^{-13}	1.90×10^{-13}
		O V (3d′ ^{3}D^0–3p′ ^{3}D)					0.76			5.87×10^{-13}
3820	3811,34	O VI (3p ^{2}P^0–3s ^{2}S)	1.0	63.8±0.44	4.64×10^{-12}	5.29×10^{-12}	1.0	336±6	9.08×10^{-13}	1.93×10^{-12}
3934	3934	C IV (6p–5s)	0.12	5.0±1.5	3.31×10^{-13}:	5.20×10^{-14}:	0.10	32.6±1.1	1.24×10^{-13}	2.60×10^{-14}
	3937	O VI (13–9)	0.76			3.29×10^{-13}:	0.80			2.08×10^{-13}
	3929	C IV (13–7)	0.12			5.20×10^{-14}:	0.10			2.60×10^{-14}
4679	4658	C IV (6–5)	0.58	90±1	2.83×10^{-12}	2.00×10^{-12}	0.47	531±4	9.71×10^{-13}	8.57×10^{-13}
	4685	C IV (8–6)	0.15			5.11×10^{-13}	0.13			2.43×10^{-13}
	4686	He II (4–3)	0.27			9.39×10^{-13}	0.40			7.42×10^{-13}
4930	4930	O V (7i–6h)	1.0	2.3±0.6	6.50×10^{-14}:	6.90×10^{-14}:	1.0	7.2±2.4	1.15×10^{-14}::	2.1×10^{-14}::
5114	5114	O V (3p ^{1}P^0–3s ^{1}S)		–	–	–	?	23±6	3.0×10^{-14}:	5.40×10^{-14}:
	5093	C IV (15–8)								
	5084	O VI (8d–7p)								
5290	5290	O VI (8–7)	1.0	9.9±0.4	2.69×10^{-13}	3.06×10^{-13}	1.0	45±2	5.04×10^{-14}	8.88×10^{-14}
5411	5411	He II (7–4)	0.5::	4±2	7.5×10^{-14}::	3.04×10^{-14}::	0.34	65±2	7.38×10^{-14}	4.31×10^{-14}
	5411	C IV (14–8)	0.5::			3.96×10^{-14}::	0.14			1.74×10^{-14}
	5470	C IV (10–7)	–				0.52			6.79×10^{-14}
5590	5590	O V (3d ^{3}D–3p ^{3}P^0)	1.0	24.5±0.3	4.78×10^{-13}	5.72×10^{-13}	1.0	112±3	1.28×10^{-13}	2.11×10^{-13}
5800	5801,12	C IV (3p ^{2}P^0–3s ^{2}S)	1.0	216±6	2.82×10^{-12}	3.26×10^{-12}	1.0	2450±190	2.22×10^{-12}	3.59×10^{-12}
6200	6200	O VI (13–10,11–9)		–	–	–	1.0	12±2	9.43×10^{-15}:	1.47×10^{-14}:
6560	6560	He II (6–4)		–	–	–	0.73	93±3	7.51×10^{-14}	8.21×10^{-14}
	6560	C IV (12–8)					0.27			3.10×10^{-14}
7062	7062	C IV (9–7)		–	–	–	1.0	102±5	6.19×10^{-14}	8.95×10^{-14}

Notes: [a] other O IV multiplets included in λ3400 blend: 3p′ ^{4}D–3s′ ^{4}P^0; 3p′ ^{2}D–3s′ ^{2}P^0; 3d′ ^{4}P^0–3p′ ^{4}S; 3p″ ^{2}D–3s″ ^{2}P^0

Table 5. Optical and infrared equivalent widths, observed (F) and dereddened (I) line fluxes and fractional line contributions, for Sand 4[a] and Sand 5

			Sand 4				Sand 5			
λ_{obs} (Å)	λ_{id} (Å)	Transition ID's	frac	EW (Å)	F (ergs cm^{-2} s^{-1})	I (ergs cm^{-2} s^{-1})	frac	EW (Å)	F (ergs cm^{-2} s^{-1})	I (ergs cm^{-2} s^{-1})
3434	3434,38	O VI (7–6,11–8)	1.0	120±8	2.29×10^{-13}	1.56×10^{-10}	1.0	75±15	2.0×10^{-13}	5.05×10^{-10}
3820	3811,34	O VI (3p ^{2}P^0–3s ^{2}S)	1.0	1524±54	4.11×10^{-12}	1.70×10^{-09}	1.0	1005±17	4.61×10^{-12}	5.30×10^{-09}
4500	4500	O V + O VI (see text)	1.0	75±7	1.97×10^{-13}	3.89×10^{-11}	1.0	43±5	2.88×10^{-13}	1.31×10^{-10}
4679	4658	C IV (6–5)	0.49	252±4	1.59×10^{-12}	1.26×10^{-10}	0.52	496±7	3.53×10^{-12}	7.33×10^{-10}
	4685	C IV (8–6)	0.14			3.59×10^{-11}	0.13			1.90×10^{-10}
	4686	He II (4–3)	0.37			9.41×10^{-11}	0.35			4.97×10^{-10}
5290	5290	O VI (8–7)	1.0	94±5	3.79×10^{-13}	2.93×10^{-11}	1.0	85±5	9.96×10^{-13}	1.55×10^{-10}
5411	5411	He II (7–4)	0.63	25±4	9.51×10^{-14}	3.89×10^{-12}	0.55	74±5	1.68×10^{-12}	5.04×10^{-11}
	5411	C IV (14–8)	0.37			2.30×10^{-12}	0.12			1.77×10^{-11}
	5470	C IV (10–7)	–				0.53			7.41×10^{-11}
5590	5590	O V (3d ^{3}D–3p ^{3}P^0)	1.0	186±7	8.62×10^{-13}	4.91×10^{-11}	1.0	222±10	3.31×10^{-12}	3.84×10^{-10}
5800	5801,12	C IV (3p ^{2}P^0–3s ^{2}S)	1.0	184±8	9.23×10^{-13}	4.41×10^{-11}	1.0	374±10	6.39×10^{-12}	6.15×10^{-10}
6200	6200	O VI (11–9,13–10)	1.0	32±4	1.8×10^{-13}	6.37×10^{-12}	1.0	40±4	5.47×10^{-13}	4.20×10^{-11}
6560	6478	O V (10–8)	0.0	115±7	6.99×10^{-13}	0	0.1:	182±5	2.77×10^{-12}	1.26×10^{-11}:
	6560	He II (6–4)	0.70			1.34×10^{-11}	0.61			7.69×10^{-11}
	6560	C IV (12–8)	0.30			5.64×10^{-12}	0.29			3.61×10^{-11}
7062	7062	C IV (9–7)	1.0	119±4	8.19×10^{-13}	1.59×10^{-11}	1.0	96±8	3.34×10^{-12}	9.46×10^{-11}
7730	7726	C IV (7–6)	0.86	400±20	2.60×10^{-12}	3.52×10^{-11}	0.86	470±80	1.50×10^{-11}	2.43×10^{-10}
	7736	C IV (11–8)	0.1				0.1			
	7860	C IV (14–9)	0.04				0.04			
1.19μm	1.184μm	O VI (3d–3p)	?	510	5.5×10^{-12}	1.9×10^{-11}				
	1.190μm	C IV (8–7)	?							
	1.193μm	O V (12–10)	<0.1							
1.55μm	1.554μm	O V (10–9,13–11)	1.0	155	1.4×10^{-12}	2.9×10^{-12}				
1.73μm	1.736μm	C IV (9–8)	1.0	750	6.0×10^{-12}	1.1×10^{-11}				
2.10μm	2.100μm	O V (11–10)	1.0	400	5.3×10^{-13}	8.2×10^{-13}				
2.43μm	2.427μm	C IV (10–9,13–11)	1.0	1550	4.3×10^{-12}	5.9×10^{-12}				

Notes: [a] IR fluxes from Dopita et al. (1990) (see text).

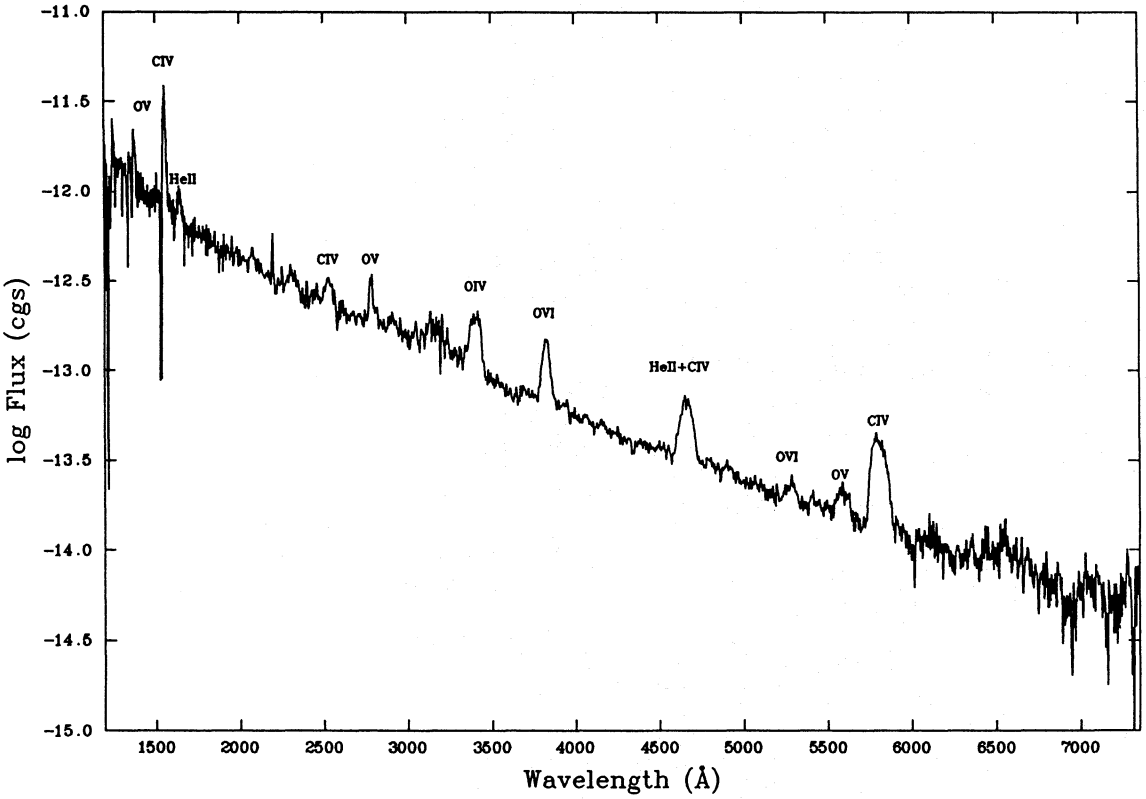

Fig. 1. The dereddened ultraviolet and optical energy distribution of Sand 1, with the strongest features identified

Table 6. Equivalent width (in Å) of emission features for MS 4 and DR 1

λ (Å)	ID	EW(MS 4)	EW(DR 1)
3400	O IV (3d ^{2}D–3p ^{2}P^0), O VI (7–6,11–8)	14	204
3811,34	O VI (3p ^{2}P^0–3s ^{2}S)	15	360
4658,86	C IV (6–5,8–6), He II (4–3)	62	330
5290	O VI (8–7)	3.5::	54:
5590	O V (3d ^{3}D–3p ^{3}P^0)	18	120:
5801,12	C IV (3p ^{2}P^0–3s ^{2}S)	170	690

the same stars. The observed optical and infrared emission line EW's and fluxes (F) for Sand 4 and Sand 5 are listed in Table 5. The equivalent widths listed in Tables 3–5 represent a weighted average of the values measured from the individual spectra, while the dereddened line fluxes (I) that are listed correspond to those measured from the final flux-calibrated spectrum created for each star, dereddened as described in Sect. 5. The identifications of the ionic transitions and their estimated fractional contribution (frac) to each emission feature are also given in Tables 3–5. The derivation of each ion's fractional contribution to a given feature is discussed in Sect. 8.2. The EW's of the strongest lines in the optical spectrum of MS 4 are presented in Table 6. The S/N and wavelength coverage of these spectra only permitted classification and terminal velocity information to be obtained; a full abundance analysis was not possible. Table 6 also presents the equivalent widths of the strongest emission lines in the spectrum of DR 1, corrected for the nebular continuum as described by Kingsburgh & Barlow (1995). Figure 1 shows the merged UV and optical spectrum of Sand 1 (a WO4 star), with the strongest features identified. The fluxes and EWs of the WO emission lines for Sand 1 and MS 4 were corrected for the presence of absorption features arising from their companion O-type stars, which could be clearly seen in the spectra.

2.4. The infrared spectrum of Sand 4

We have derived infrared line fluxes from the 1–2.5 μm spectrum of Sand 4 published by Dopita et al. (1990). Their small-aperture spectrum was traced and placed on an absolute scale by convolving it with UKIRT J, H and K filter profiles, to obtain synthetic J, H and K magnitudes. The scaling factors needed to put the three regions of the spectrum on an absolute scale were then ob-

Table 7. Original WO classification scheme of Barlow & Hummer (1982)

WO Subtype	Criteria
WO1	no O IV; O V > C IV
WO2	no O IV; O V < C IV
WO3	O VI > O IV; O V < C IV
WO4	O VI < O IV; O V < C IV

tained by comparing these synthetic magnitudes with UKIRT J, H and K photometry of Sand 4 kindly provided by Dr. P.M. Williams (private communication). The final line fluxes are thus on an absolute scale. The resulting line fluxes are presented in Table 5.

3. The WO classification scheme

3.1. Classification criteria

Table 7 presents the original WO classification scheme of Barlow & Hummer (1982). The original scheme was based on the relative strengths of the O IV 3400 Å and O VI 3811,34 Å lines for the late WO subclasses, and the relative strengths of O V 5590 Å and C IV 5801,12 Å lines for the early WO subclasses. For a definitive WO classification, spectral coverage which includes all four aforementioned features is required. Unfortunately, published spectral coverage often does not extend below 4000 Å and is therefore not adequate for the WO classification scheme of Barlow & Hummer to be used properly. Smith et al. (1990b) proposed separating WO from WC stars by requiring that for WO stars the line width (FWHM) of the C IV 5801,12 Å feature be larger than 90 Å, as well as larger than that of the C IV + He II (+C III in the WC subtypes) 4658–86 Å feature. Smith & Maeder (1991) proposed five WO candidates in M 33 based on these criteria. However, spectroscopy of WR stars in M 33 by Willis et al. (1992), which included the 3800 Å region, has shown that three of Smith & Maeder's WO candidates, MC 6, MC 48 and MC 78, lack strong O VI emission and cannot be WO stars (the other two WO candidates of Smith & Maeder 1991 were not observed by Willis et al.). Willis et al. found that MC 6 was a WC4-5 star, while MC 48 and MC 78 were WC4 stars.

We present here a quantified scheme for WO classification, as an extension to the original scheme of Barlow & Hummer. The details of this scheme are presented in Table 8. Since the original scheme is sensitive to the C/O abundance ratio, we have added criteria relating the strengths of the O V 5590 Åand O VI 3811,34 Å features, which originate from the same element, which can be used alone to define the WO subclass when spectral coverage is limited. However, the intervals in the the O VI to O V equivalent width ratio (Table 8) that correspond to a change of one subtype ($\sim$ 0.2 dex) are much smaller than for the O VI to C IV equivalent width ratio ($\sim$ 0.5 dex), making the latter ratio preferable for spectral typing, with the former ratio serving as a backup. We have extended the original WO sequence to include a lower excitation WO5 subclass, which has EW(O VI 3811,34)/EW(O V 5590) $\sim$ 1, compared to the ratio of about 3 found for WO4 stars. As described below, this new subtype has been applied to MS 4. The absence or presence of C III λ5696 emission can be used to discriminate between WO stars and WC4 stars, respectively.

The equivalent widths of the strongest stellar emission line features in the spectrum of DR 1, after subtraction of the underlying nebular continuum (as described by Kingsburgh & Barlow 1995), are presented in Table 6. Using these values and the classification criteria of Table 8, we derive a spectral type of WO3 for DR 1, making it the first member of this subclass. If the nebular continuum had not been subtracted, a later (WO4) subclass would have been derived for DR 1.

3.2. The WO5 component of MS 4

MS 4 is a heavily reddened WR star (in the direction of the Carina Arm) with an O-type companion. Moffat & Seggewiss (1984) classified it as a WC4 + O4 system. Smith et al. (1990a) re-classified it as a WO4 + O4 system. However, the spectra used for both previous classifications did not include the 3400 Å region. The emission line measurements from our spectra of MS 4 (Table 6; allowance has been made for the presence of the O-star's photospheric lines in the profiles of some of the WO star's emission lines) show that EW(O IV 3400) $\simeq$ EW(O VI 3811,34), which on the original Barlow & Hummer (1982) classification scheme would give it a WO4 type. However, in the spectra of the WO4 stars Sand 1 and Sand 2, EW(O VI 3811, 34) $\simeq$ 3 $\times$ EW(O V 5590), whereas in the spectrum of MS 4, EW(O VI 3811, 34) $\simeq$ EW(O V 5590). The excitation of MS 4 is therefore clearly lower than that of the WO4 stars Sand 1 and Sand 2, but higher than that found for WC4 stars. Although WC4 stars show a range of O VI/O V ratios (Smith et al. 1990a) that encompass that of MS 4, unlike MS4 and the other WO stars WC4 stars show C III λ5696 emission. This led us to define the new WO5 class (Table 8), into which we place MS 4. Since we found that the equivalent width ratio of O VI 3811,34 Å to C IV 5801,12 Å was also lower for MS 4 than for the WO4 stars Sand 1 and Sand 2, this ratio can also be used as a defining criterion to separate WO4 stars from WO5 stars (see Table 8).

Rustamov & Cherepaschuk (1987) have proposed their own WO5 classification, for early-WC stars which show some O VI 3811,34 Å emission and which also show C III 5696 Å emission. Their WO5 criteria encompassed a number of stars in the WC4–6 classes. Since the stars in question have weaker O VI emission lines than the WO stars discussed here, and since they otherwise fit fairly easily into the normal WC classification scheme, we prefer here to reserve the WO classification for those stars that cannot easily be fitted into the WC scheme, in particular those which show strong O VI 3811,34 emission but which do not show C III λ5696 emission.

Table 8. Revised WO spectral classification

Subtype	$\log \frac{EW(O\ VI)}{EW(C\ IV)}$	$\log \frac{EW(O\ VI)}{EW(O\ V)}$	Other Criteria	Members
WO1	> 0.7	> 0.8	no O IV; O V $\gtrsim$ C IV	Sand 4
WO2	$0.1 \rightarrow 0.7$	$0.65 \rightarrow 0.8$	no O IV; O V < C IV	Sand 5
WO3	$-0.4 \rightarrow 0.1$	$0.48 \rightarrow 0.65$	O IV < O VI; O V << C IV	DR 1
WO4	$-0.9 \rightarrow -0.4$	$0.25 \rightarrow 0.48$	O IV $\simeq$ O VI; O V << C IV	Sand 1, Sand 2
WO5	< -0.9	< 0.25	O IV > O VI; O V << C IV	MS 4

Notes to Tables 7 and 8:

Wavelengths of lines used in classification: O IV 3400 Å, O VI 3811,34 Å, O V 5590 Å and C IV 5801,12 Å.

All WO stars have strong C IV 5801,12 Å and no lines of C III.

Table 9. Absorption line equivalent widths for the O-type components of Sand 1 and MS 4

λ	ID	Sand 1 EW(Å)	MS 4 EW(Å)
3750	H 12	0.48	–
3770	H 11	1.21	–
3798	H 10	–	0.72
3835	H 9	–	0.47
3889	H 8, He I	1.15	1.43
3934	IS Ca II K	–	0.95
3970	H 7, IS Ca II H	2.36	2.43
4026	He I, He II	0.45	0.74
4101	Hδ	1.09	1.48
4200	He II	0.40	0.75
4340	Hγ	1.10	1.70
4430	IS DIB	–	4.72
4471	He I	0.39	0.2:
4542	He II	0.44	0.80
4861	Hβ	–	2.49
5411	He II	–	1.03
5780	IS DIB	–	1.20
5890	IS Na I D2	–	1.22
5896	IS Na I D1	–	0.82
Spectral	Type	O7	O4

4. Companion star spectral types

4.1. The O-star component of Sand 1

The absorption line equivalent widths measured for the O-type component of Sand 1 are presented in Table 9. A discrepancy exists in the literature for the spectral type of this O-type companion. Barlow & Hummer (1982) classified it as O7. However Moffat et al. (1985) argued for an O4 spectral type on the basis of their observation of log (EW(He I 4471)/EW(He II 4542)) = −0.52. In our three medium resolution AAT spectra, the equivalent width ratio of He I λ4471 to He II λ 4542 was found to be consistent between each of the spectra, with a mean log (EW(He I)/EW(He II)) = -0.05 ± 0.13. From the O-type classification scheme of Conti & Altschuler (1971), this EW ratio indicates that the O star component of Sand 1 is an O7(±0.5) star (see Fig. 2). The same log(EW) ratio for an O4 star is −0.6. The lines which are normally used for the Of classification of O-stars, namely He II λ4686 and N III λλ4634,40, are completely swamped by the WO star's emission lines in this case.

The luminosity classification lines, Si IV λλ4089, 4116 and He I λ4143, were too weak to be detected. We can estimate the luminosity class of this O7 star by adopting the absolute visual magnitude of −2.5 derived for the WO4 star Sand 2 (see Sect. 5) as appropriate for the WO4 component of Sand 1, on which basis one obtains $M_V = -5.5$ for the O7 star. According to Howarth & Prinja (1989), the M_V for an O7III star is −5.6, while the M_V for an O7V star is −4.9. Our derived M_V for the O7 component of Sand 1 makes it most likely to be a giant, but higher signal to noise spectra, to detect the luminosity classification lines, are needed to confirm this.

The orbital parameters of Sand 1 have been derived from spectropolarimetry by Moffat et al. (1991), who derived a period of 16.6 days, an eccentricity of zero, $M(\mathrm{WO}) \sin^3 i = 3.9\,\mathrm{M}_\odot$ and $M(\mathrm{O}) \sin^3 i = 14.5\,\mathrm{M}_\odot$. The inclination derived by Moffat et al. was 112°, hence their derived mass for the O7 star was

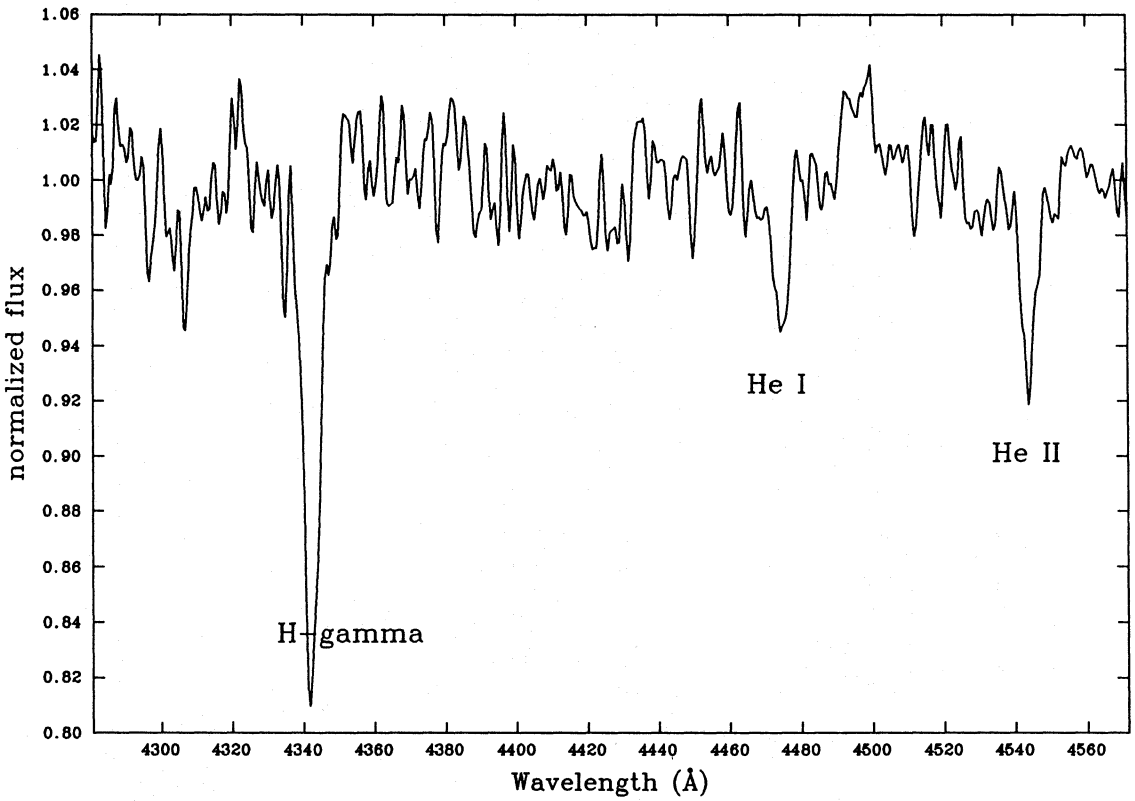

Fig. 2. A portion of the optical spectrum of Sand 1, with the continuum normalized to unity. The ratio of the He I 4471 Å to He II 4542 Å absorption lines yields a spectral class of O7(±0.5) for the O-type primary (see Sect. 4.1)

18 $M_\odot$, while the corresponding mass derived for the WO4 star was 5 $M_\odot$.

4.2. The O-star component of MS 4

The O-star absorption line EW's measured in our AAT service spectrum of MS 4 are presented in Table 9. The EW of He I λ4471 is uncertain, due to insufficient S/N in the spectrum. The weakness (or perhaps lack) of this line relative to He II λ4542 gives a limit on the O-star spectral type as $\leq$ O5, consistent with the results of Moffat & Seggewiss (1984), who derived an O4 type. The luminosity class is difficult to estimate, as in the case of Sand 1 above.

5. Reddenings, magnitudes and distances

Reddenings to Wolf–Rayet stars can be difficult to determine. Morris et al. (1993) have derived reddenings to Galactic and Magellanic Cloud WN and WC stars by a combination of the nulling of the 2200 Å extinction feature and imposing the requirement that the overall dereddened UV-optical continuum energy distributions be fitted by power-laws. On this basis, they found that the majority of WN and WC stars had power-law slopes (F_λ vs. λ) of -3 (compared to -4 given by a Rayleigh-Jeans distribution). Morris et al. also noted that recently calculated model atmospheres for WR stars (e.g. Wessolowski et al. 1989, Schmutz et al. 1992) produced UV-optical energy distributions which could be approximated by power-law slopes of -3. The planetary nebula central star Sand 3 has a high-excitation emission line spectrum which resembles those of the Population I WO stars more closely than do the spectra of the Population I WN and WC stars. Barlow & Hummer (1982) showed that nulling the 2200 Å extinction feature towards Sand 3 yielded an optical-UV energy distribution that could only be fitted by the Rayleigh-Jeans tall of blackbodies with temperatures in excess of 10^5 K, i.e. a power-law with a slope of -4. Based on photoionization modelling of G 2.4+1.4, the nebula surrounding the WO1 star Sand 4, using blackbody models, Dopita et al. (1990) estimated a stellar effective temperature of about 1.5 10^5 K, while Esteban et al. (1993), using the Wolf–Rayet model atmospheres of Schmutz et al. (1989), derived an effective temperature of 105 000 K for Sand 4. In order to check what the intrinsic continuum energy distribution of a WO-like star should look like, Dr. P.A. Crowther kindly calculated a model, using the code described by Hillier (1989), with the following parameters: $T_* = 10^5$ K, $R_* = 1.5 R_\odot$, $M_V = -2.7$, $4.5\,10^{-5}\,M_\odot\ \mathrm{yr}^{-1}$, $v_\infty = 4500\,\mathrm{km\,s}^{-1}$, and C/He = 0.5 and O/He = 0.15, by number. The overall 0.12–1.0μm energy distribution of this model could be approximated by a power-law of slope -3.1. We therefore make the assumption here that all the *single* WO star systems have intrinsic energy distributions that are close to power-laws of slope -3 in the observable ultraviolet and optical regions.

Table 10. WO star parameters

	Sand 1	Sand 2	Sand 4	Sand 5	MS 4
a.k.a.	Sk 188, AB 8	Brey 93, FD 73	WR 102	WR 142, St 3	WR 30a
Class	WO4 + O7	WO4	WO1	WO2	WO5 + O4
V	13.33	16.37	14.56	13.37	12.80
B–V	–0.26	–0.03	1.33	1.72	1.00
E(B-V)	0.02(galactic)	0.08(galactic)	1.45	1.70	1.32
	0.03(SMC)	0.10(LMC)			
D (kpc)	57.5	46.8	(2.3)	0.95	(8.7)
M_V	–5.6	–2.5	(–1.8)	–1.8	(–6.0)
v_∞ (km sec^{-1})	4200±50	4500±400	4600±200	5500±200	4500±400

The reddenings towards stars in the Magellanic Clouds are in general low. The reddening, $E(B-V)$, for the SMC WO4+O7 binary Sand 1 was derived by the following method, used by Barlow (1987) to estimate reddenings towards Magellanic Cloud planetary nebulae: (i) the foreground galactic component of $E(B-V)$ was determined using the galactic reddening map of Burstein & Heiles (1982), which gave $E(B-V) = 0.02$. Its spectrum was dereddened adopting this value of $E(B-V)$ and the galactic optical and UV reddening functions of Howarth (1983) and Seaton (1979); (ii) the component of $E(B-V)$ due to the SMC was obtained from the map of N(H I) for the SMC published by Hindman (1967; via his Fig. 2), and the application of Fitzpatrick's (1985) determination of $N(\mathrm{H\,I})/E(B-V) = 8.7\,10^{22}\,\mathrm{cm}^{-2}\mathrm{mag}^{-1}$ for the SMC, with the assumption that Sand 1 is located halfway along the SMC dust column; with this method the SMC $E(B-V) = 0.03$. The spectrum was then further dereddened using this value of $E(B-V)$ and Prevot et al.'s (1984) SMC reddening law.

For all of the WO stars, stellar *continuum* B and V magnitudes were derived from the interpolated wide-slit continuum fluxes at 4400 Å and 5470 Å, respectively, where we adopted zero-magnitude flux calibrations of 4380 Jy for B and 3694 Jy for V. The measured continuum V magnitudes and $(B-V)$ colours are presented in Table 10. From Table 10, the overall $E(B-V)$ of 0.05 towards Sand 1, derived above, implies a dereddened continuum $(B-V)_0$ of -0.31 for it, consistent with the intrinsic colour expected for the O7 primary which dominates its continuum energy distribution.

For Sand 2, a similar procedure to that described above for Sand 1 was used to estimate a foreground galactic reddening component of $E(B-V) = 0.08$, and the LMC reddening component was estimated using the $N(\mathrm{H\,I})$ versus position table of Rohlfs et al. (1984), with the adoption $N(\mathrm{H\,I})/E(B-V) = 2\,10^{22}\,\mathrm{cm}^{-2}\,\mathrm{mag}^{-1}$ for the LMC (Koornneef 1982). This yields $E(B-V) = 0.22$ for the total LMC dust column in the direction of Sand 2. The assumption that Sand 2 is halfway along the LMC dust column would therefore imply an LMC reddening component of $E(B-V) = 0.11$. The observed ultraviolet-optical spectrum of Sand 2 was dereddened first with the galactic reddening component of $E(B-V) = 0.08$ and then further dereddened by varying amounts using Fitzpatrick's (1985) 30 Doradus reddening law as the appropriate one for Sand 2's location in the LMC. An LMC $E(B-V)$ of 0.10 (in addition to the Galactic $E(B-V)$ of 0.08) was found to yield a dereddened UV-optical continuum which could be approximated by a power-law of -3.04. We therefore adopted $E(B-V) = 0.10$ for the LMC reddening component.

For the heavily reddened galactic WO stars Sand 4 and Sand 5, we derived the reddening from the the observed optical continuum slopes. For Sand 4, it was found that dereddening by $E(B-V) = 1.45$ yielded an optical continuum slope of -3.07, so this value for the reddening was adopted, corresponding to $A_V = 4.50$ for $R = 3.1$. For Sand 5, there was some concern as to the accuracy of the magnitudes that could be derived from our wide-slit spectrophotometry, due to the large zenith distance to this star from the AAT. We therefore convolved our spectrophotometry of this star with the B and V filter profile functions given by Lamla (1982) and ratioed the resulting in-band fluxes with those derived by applying the same procedure to the tailored Kurucz (1991) model atmosphere for Vega that is described by Cohen et al. (1992), where Vega was adopted to have $V = 0.03$ and. $(B-V) = 0.00$, plus a 5556 Å flux of 3540 Jy. The resulting magnitudes derived from our AAT spectrophotometry of Sand 5 (*including* the stellar emission lines) were $B = 14.36$ and $V = 12.88$, which can be compared with the photoelectric magnitudes of $B = 14.39$ and $V = 12.96$ obtained by Turner & Forbes (1982). The relatively good agreement between these B and V measurements gives us confidence as to the reliability of the underlying continuum magnitudes of $B = 15.09$ and $V = 13.37$ that we derive from our spectrophotometry of Sand 5. We dereddened the observed energy distribution of Sand 4 with various values of $E(B-V)$ and found that an $E(B-V)$ of 1.70 yielded a dereddened optical continuum energy distribution which could be approximated by a power-law of slope -3.02. This reddening agrees well with the $E(B-V)$ of 1.70 ± 0.1 estimated by Turner & Forbes (1982) for the direction to Sand 5, from the reddenings measured towards surrounding stars in

Table 11. Ultraviolet P Cygni absorption velocities (km s^{-1})

	Sand 1	Sand 2
O v 1371	2450±150	3100±300
C iv 1548,50	4200±50	4500±400

the cluster. We therefore adopted $E(B-V) = 1.70$ for Sand 5, corresponding to $A_V = 5.27$.

Our wide-slit spectrophotometry of the WO5+O4 binary MS 4 yields continuum magnitudes of $B = 13.80$ and $V = 12.80$. The implied $E(B-V)$ of 1.32 is in excellent agreement with the E_{b-v} of 1.09 estimated for MS 4 by Smith et al. (1990a), which for $E(B-V) = 1.21E_{b-v}$ (Turner 1982), also yields $E(B-V) = 1.32$. For $R = 3.1$, $A_V = 4.09$.

Our derived magnitudes and distances are presented in Table 10. The distances to Sand 1, Sand 2 and Sand 5 are independently known, from their memberships of the SMC, the LMC and the galactic open cluster Be 87, respectively, so absolute magnitudes can be derived for them. Table 10 lists the continuum B and V magnitudes derived for each star, along with the adopted reddenings. For Sand 1, the adoption of a distance modulus of 18.8 for the SMC (Reid & Strugnell 1986) gives $M_V = -5.6$ for this O7 + WO4 system. For Sand 2, a distance modulus of 18.35 for the LMC (Reid & Strugnell 1986) gives $M_V = -2.5$. For Sand 5, a distance of 0.95 kpc is adopted from its membership of the open cluster Be 87, for which Turner & Forbes (1982) derived a distance modulus of 9.88. The resulting continuum absolute magnitude for Sand 5 is $M_V = -1.8$. Since the WO1 star Sand 4 does not have an independent distance estimator, we have adopted the M_V derived for the WO2 star Sand 5 to estimate a distance of 2.3 kpc for Sand 4. For the O4 + WO5 system MS 4 (WR 30a) we adopt the same absolute magnitude of $M_V = -6.0$ as Moffat & Seggewiss (1984), which yields a distance of 8.7 kpc.

From Table 10, we see that the reddenings derived for the WO stars decrease with increasing distance, the closest WO star having the highest reddening and the furthest WO star having the lowest reddening. Selection effects clearly determine this behaviour, since highly reddened WO stars are only likely to be discovered if they are nearby while very distant WO stars are only likely to be discovered if they have low reddenings.

6. Wind expansion velocities

6.1. Ultraviolet P Cygni absorption velocities

The strongest line present in the ultraviolet spectrum of Sand 1 is the C IV 1548,50 Å resonance doublet, whose P Cygni black absorption edge was used to determine the terminal velocity of the wind from the WO component of Sand 1. Following the method of Prinja et al. (1990), a terminal velocity (v_∞) of 4200 km s^{-1} was obtained from the blue limit of zero residual intensity in the saturated C IV 1548,50 Å profile (i.e. $v_{\rm black}$ – see Fig. 3), in agreement with the estimate of Barlow & Hummer (1982). Å number of interstellar absorption lines shortward of O IV 1343 Å and O V 1371 Å make the presence of P Cygni profiles in these two lines difficult to discern in the low resolution spectra. Fortunately, in the high resolution spectrum of Sand 1, the interstellar features were clearly resolved; O IV 1343 Å is a pure stellar emission line, whilst O V 1371 Å shows definite P Cygni structure. Interstellar absorption lines of C II1334.5 Å and C II* 1335.3 Å are quite strong in the high resolution spectrum and blend together in the low resolution spectra of Sand 1, giving O IV λ1343 Å the misleading appearance of a P Cygni profile (see Fig. 4). Since similar O IV 1343 Å profiles occur in the low resolution *IUE* SWP spectrum of Sand 2, we again assumed O IV λ1343 to be pure emission and O V λ1371 to have a P Cyg profile. For O V λ1371 in Sand 1, $v_{\rm exp}$ was measured as the deepest blue point in the high resolution spectrum. For Sand 2, only low resolution SWP spectra were available and the $v_{\rm exp}$ velocities for C IV 1548,50 Å and O V 1371 Å were taken to be halfway between $v_{\rm deepest}$ and $v_{\rm edge}$. In the case of Sand 2, the terminal velocity was taken to be equal to the value of $v_{\rm black}$ derived from C IV 1548,50 Å. Expansion velocities derived from the various ultraviolet lines are given in Table 11.

The N V 1238,42 Å resonance doublet is present in the *IUE* spectrum of Sand 1 (WO4 + O7) – see Fig. 5, but is not present in the spectrum of Sand 2 (WO4). Lines of nitrogen are not seen in the spectra of eaxly WC stars nor in those of the other WO stars. Thus we interpret this N v feature as arising from the O-star component of Sand 1, and used it to derive its wind terminal velocity. The deepest blue point in the high resolution spectrum of this line yields a terminal velocity of 2140 km s^{-1} which is consistent with the terminal velocities derived for O7 stars by Prinja et al. (1990).

6.2. UV and optical emission line width velocities

The full width at zero intensity (FWZI) and full width at half maximum (FWHM) were measured for all emission lines. The widths were then corrected for the instrumental profile (in quadrature) and for any doublet or multiplet separation, then converted to expansion velocities, $v_{\rm exp}$. It was assumed that the line FWHM was equal to $v_{\rm exp}$ and that the FWZI was equal to twice $v_{\rm exp}$. The measured values of FWHM, FWZI/2 and the corrected $v_{\rm exp}$ are presented in Table 12. General agreement was found between the values of $v_{\rm exp}$ derived from a line's FWHM and from its FWZI/2. For some lines (e.g. O VI 5290 Å and O V 5590 Å), blending with other lines causes greater uncertainty in measuring the FWZI compared to the FWHM.

For WR stars, it can be difficult to decide which lines' $v_{\rm exp}$ best represent v_∞, since lines can be severely blended. In order to decide which of the optical emission line widths were most representative of v_∞, the expansion velocities, $v_{\rm exp}$, derived from optical emission lines in the spectrum of Sand 1 were compared to the value of $v_{\rm black}$ from C IV 1548,50 A. Inspection of Table 12 reveals that the expansion velocity of 4150 km s^{-1} given by the FWZI/2 of C IV 5801,12 Å gives the best agreement with the λ1549 $v_{\rm black}$ of 4200 km s^{-1}, so the C IV 5801,12 Å FWZI/2 (corrected for doublet separation) was

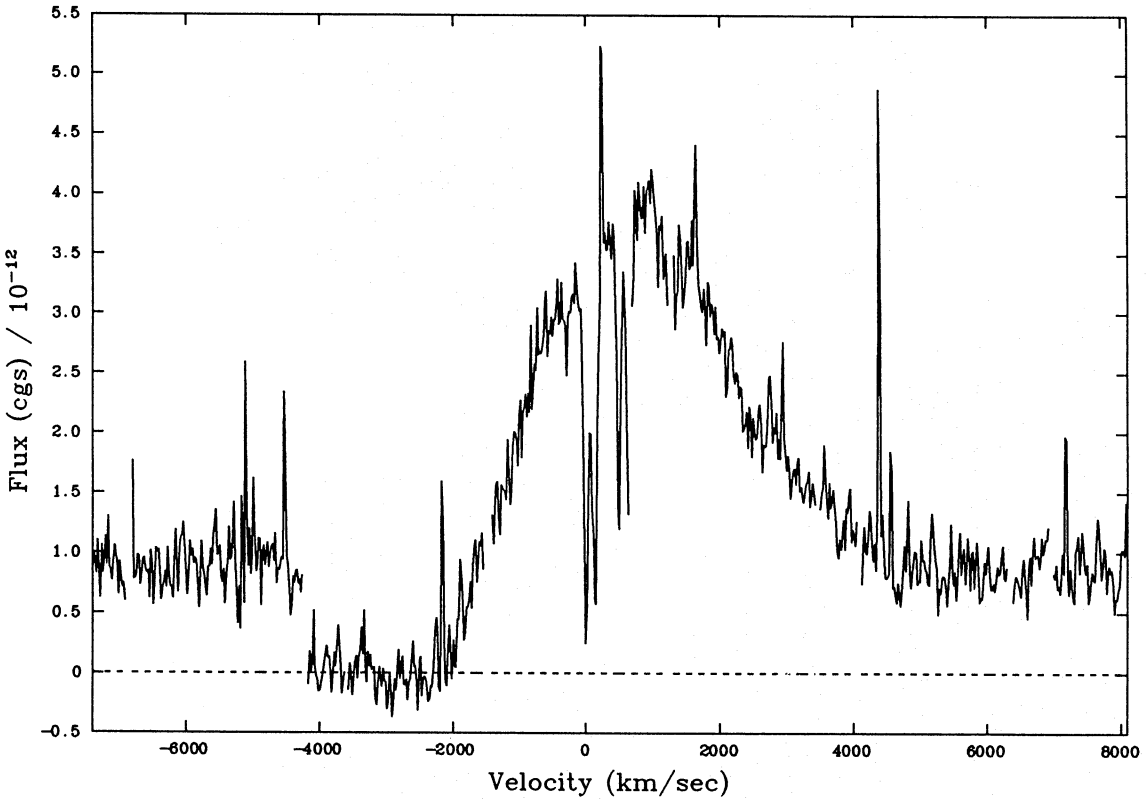

Fig. 3. The C IV 1548,1550 Å resonance doublet profile of the WO4 component of Sand 1. The violet edge of the fully saturated absorption, $V_{\rm black}$, yields a terminal velocity of 4200 km s^{-1}

used to derive v_∞ for the other WO stars. For Sand 2, the FWZI/2 of 4450 km s^{-1} of C IV 5801,12 Å agreed with the $v_{\rm exp}$ of 4500 km s^{-1} derived from C IV λ1549 in the low resolution SWP spectrum, giving support to the adoption of v_∞ as equal to the FWZI/2 of C IV 5801,12 Å for the other WO stars. Table 12 lists this quantity (corrected for the doublet separation) for Sand 4 and Sand 5, along with the various other line widths measured for those two stars. For the WO5 component of MS 4, we derived v_∞ = 4500 km s^{-1} from the FWZI/2 of C IV 5801,12 Å (corrected for the doublet separation).

Thus the galactic WO 1 star Sand 4 has a terminal velocity of 4500 km s^{-1}, while Sand 5, the galactic WO2 star, has the highest terminal velocity, 5500 km s^{-1}. The WO3 star DR 1 in IC 1613 has a terminal velocity of only 2850 km s^{-1} (Kingsburgh & Barlow 1995), and the SMC and LMC WO4 stars, Sand 1 and Sand 2, have terminal velocities of 4200 km s^{-1} and 4500 km s^{-1}, respectively, while the galactic WO5 star MS 4 has v_∞ = 4500 km s^{-1}. There is therefore no apparent trend of increasing terminal velocity with earlier WO spectral type, such as is loosely present for galactic WN and WC subtypes (e.g. Howarth & Schmutz 1992). The lowest wind terminal velodties, those of DR 1 and Sand 1, are found for the WO stars located in the lowest metallicity galaxies.

7. Some spectral characteristics of the WO stars

Tables 3, 4 and 5 list fluxes for well-known lines of He II, O IV, O V, O VI and C IV measured in our ultraviolet and optical WO star spectra. In addition to these lines, a number of weaker features are also present. Sand 4 (WO1) has the highest excitation spectrum of the sample. Barlow & Hummer (1982) noted the presence of a feature at 6068 Å in the spectrum of Sand 4, which they attributed to O VIII 10–9 λ6068.6 and 13–11 λ6064.4. This feature was also noted by Dopita et al. (1990) and by Polcaro et al. (1992) and can be seen in the spectral plots of Sand 4 which they presented. O VII 12–10 λ6084.8 may also contribute to the wing of the feature. The spectrum of Sand 4 presented by Polcaro et al. shows the 6068 Å feature to be narrower than others in the spectrum, consistent with its formation at the bottom of the wind. The expected O VIII 9–8 line at 4340.8 Å, which was seen by Barlow et al. (1980) in the spectrum of the planetary nebula nucleus Sand 3, is blended with a stronger He II 10–4 line in the case of Sand 4, while the O VIII 11–10 line at 8202 Å is blended with O VII 3p ^{1}P – 3s ^{1}S λ8241.7 and with O VI 12–10 λ8282, in a broad feature that we observe to extend from 8180–8320 Å.

The 8–7 and 9–8 lines of O VII, at 3887.1 Å and 5669.6 Å, were observed in the spectrum of Sand 3 by Barlow et al. (1980) but, due to the higher wind velocities and broader lines of Sand 4 and 5, the O VII 8–7 line is lost in the wing of the very strong O VI 3811,34 Å doublet, while the 9–8 line is engulfed in the overlap between O V λ5590 and C IV λ5805. However, we do

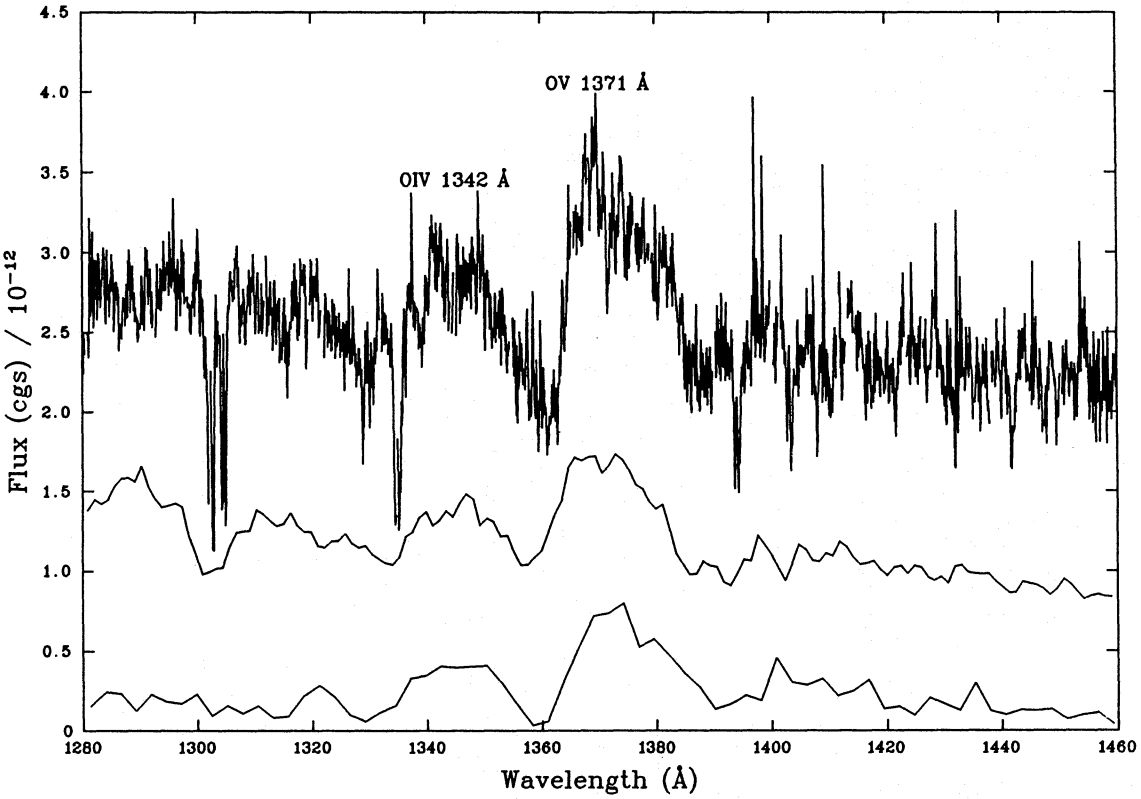

Fig. 4. The top spectrum shows the high resolution *IUE* SWP spectrum of Sand 1. The middle and lower spectra show the summed low resolution spectra of Sand 1 and Sand 2, respectively. The interstellar C II 1334.5 Å and C II* 1335.3 Å absorption lines, seen clearly in the high resolution spectrum of Sand 1, mimic a P Cygni absorption profile for O IV 1343 Å in the low resolution *IUE* spectra

see a relatively narrow feature due to O VII 10–9 λ7926.3 in the spectrum of Sand 5.

As well as the strong O V 3d ^{3}D – 3p ^{3}P λ5590 multiplet and 3p ^{3}P^0 – 3s ^{3}S λ2786 multiplet, a number of other O V transitions are observed in the WO-star spectra. The 3p ^{1}P^0 – 3s ^{1}S, λ5114 (M1) transition of O V is seen in the spectra of Sand 2, 4 and 5, while a number of excited-state transitions of O V are also seen, particularly in the case of Sand 2. A prominent feature peaking at about 3700 Å (most prominently in the spectrum of Sand 2 – see Fig. 6) is too strong to be due solely to C IV 9–6 λ3690. The major contributor to this feature appears to be the O V 3d′ ^{3}D^0 – 3p′ ^{3}D M8 multiplet, extending from 3690 Å to 3762 Å. In the case of Sand 2, which has a strong O IV 3400 Å feature, the 3d′ ^{4}F^0 – 3p′ ^{4}D 3726–3758 Å M6 multiplet of O IV might also provide a significant contribution. The spectra of Sand 2, 4 and 5 exhibit a broad emission feature between 4055 and 4255 Å, which we attribute to a blend of the 3p′ ^{3}D–3s′ ^{3}P^0 4119–4178 Å M4 O V multiplet and the 3d′ ^{3}P^0 – 3p′ ^{3}S 4120–4159 Å M11 O V multiplet, with the $\lambda\lambda$4089,4116 4p ^{2}P^0 – 4s ^{2}S M1 doublet of Si IV probably also contributing. A feature extending from 4420–4575 Å in the spectra of Sand 2, 4 and 5 appears to be predominantly due to O V transitions, namely 9–7 λ4521, 7h–6g $\lambda\lambda$4447–4499 (M21 and M22), 7g ^{1}G – 6f ^{1}F^0 λ4548 (M24), 3d′ ^{1}P^0 – 3p′ ^{1}D λ4522.7 (M15), and 3d′ ^{1}D^0 – 3p′ ^{1}P λ4554.5 (M7), together with O VI 10–8 λ4499 and C IV 6d–5p λ4441.

The strength of the excited-state O V transitions in the spectra of the WO stars, particularly in the spectrum of the single WO4 star Sand 2, is probably due to recombinations of O^{6+} from its 2p ^{2}P^0 excited state. This level is connected to the 2s ^{2}S ground-state by the well known O VI resonance doublet at 1032,38 Å. Since the excitation energy of the 2p ^{2}P^0 excited state is not large, if the O VI resonance doublet, like the C IV 1548,50 Å resonance doublet, is optically thick in the winds of these stars, then significant populations can be attained in the 2p ^{2}P^0, state. For example, for a wind electron temperature of T_e = 5 10^4 K, the Boltzmann ratio for N(2p) /N(2s) is 0.185. Recombinations onto O VI $1s^2$2p will populate $2pnl = nl'$ states of O V, for which the highest bound state corresponds to $n = 5$. Therefore the $2p5l$ and lower states of O V will be populated. These will decay to to $2snl'$ and $2pn'l'(n' < 5)$ with the cascades giving rise to the observed excited state transitions of O V. The analysis of the relative intensities of the excited-state and non-excited-state transitions of O V, to obtain N(2p) /N(2s) for O VI, therefore holds some promise as a diagnostic of the electron temperature in the winds of WO stars. There will also be direct recombinations from O VI $1s^2$2p to O V $1s^2$2p^2, increasing for example the effective recombination coefficient for O V λ1371 2p^2 ^{1}D – 2s2p ^{1}P^0 above the level accounted for by standard radiative and low-temperature dielectronic recombination theory.

Table 12. Emission feature FWHM and FWZI/2 values

	Sand 1				Sand 2			
	FWHM (observed) (Å)	FWHM (corrected) (km sec^{-1})	FWZI/2 (observed) (Å)	FWZI/2 (corrected) (km sec^{-1})	FWHM (observed) (Å)	FWHM (corrected) (km sec^{-1})	FWZI/2 (observed) (Å)	FWZI/2 (corrected) (km sec^{-1})
O IV 1342	15:	2250±150	12	2250±200	17	2600±250	13	2350±300
He II 1640	24.6	4500±100	22	4000±100	23	4250±100	25	4500±100
C IV 2530	25	2240±300	24	2450±400	31	3000±350	20	4400±400
O V 2786	18	880±300	24	1970±300	20	400±400	23	1580±500
O VI 3811,34	50	2100±100	57	3550±200	59	2200±100	63	3800±200
O VI 5290	52	2950±400	51	2900±500	43	1800±400	41	2000±400
O V 5590	77	2350±150	65	2600±250	76	2000±350	63	2280±350
C IV 5801,12	106	4950±150	85	4150±100	114	5100±100	95	4450±100
O VI 6200	–		–		53::	2100±600	36	1400±600
C IV 7062	–		–		80::	3200±400	50	2000±800

	Sand 4				Sand 5			
	FWHM (observed) (Å)	FWHM (corrected) (km sec^{-1})	FWZI/2 (observed) (Å)	FWZI/2 (corrected) (km sec^{-1})	FWHM (observed) (Å)	FWHM (corrected) (km sec^{-1})	FWZI/2 (observed) (Å)	FWZI/2 (corrected) (km sec^{-1})
O VI 3434	55	4000±500	36	2600±600	50	3600±1000	30	2000±1000
O VI 3811,34	81	4150±100	79	4800±100	94	5600±200	76	4850±200
O VI 5290	83	4350±300	62	3300±300	63	3100±400	61	3250±400
O V 5590	164	6450±400	92	3950±300	160	6600±300	104	4580±350
C IV 5801,12	150	7000±300	94	4450±250	145	6750±300	115	5500±200
O VI 6200	75	3300±400	55	2500±400	99	4600±500	55	2500±500
C IV 7062	159	6600±800	144	6000±800	175	7300±600	106	4400±600

Notes to Table 12:
The 'corrected' FWHM and FWZI/2 values are corrected for instrumental resolution and doublet separation, when appropriate

In their JHK-band spectra (1.1–2.5 μm) of Sand 4, Dopita et al. (1990) attributed several observed features to C V 12–10, 10–9+13–11 and 11–10. However, since the ionization potential needed to create C^{5+} is 392 eV, versus only 114 eV to create O^{5+}, and since the corresponding O V infrared transitions have almost the same wavelengths as those of C V, it appears likely that O V makes a significant contribution to these IR features (see Sect. 8.3.3). The strongest optical line from C V is expected to be the 7i–6h transition at 4944.8 Å, only 900 km s^{-1} away from the corresponding O V transition, at 4930.3 Å. Sand 2 (WO4) exhibits a feature peaking at 4930 Å in its spectrum, which we attribute to O V 7i–6h, while Sand 4 (WO1), which exhibits O VII+O VIII emission elsewhere (see above), shows a broad emission feature extending from 4880–4895 Å, which may be due to both O V and C V. Sand 5 (WO2) has a narrower feature, extending from 4880–4955 Å, which is probably dominated by just O V.

8. Abundance analysis

8.1. Derivation of abundances in Wolf–Rayet winds

The great strength of Wolf–Rayet winds and the consequent lack of photospheric absorption lines significantly complicates most abundance analysis techniques. Detailed non-LTE models have been constructed for a few stars (e.g. Hillier 1989; Hamann et al. 1992). However, the need for large amounts of CPU time to model lines spanning a large spectral range has so far limited such analyses to only a small number of stars. The use of recombination theory to interpret the relative intensities of ionic recombination lines provides a more straightforward approach to deriving abundances, and the results from.this approach have been broadly confirmed by detailed non-LTE modelling. Hummer et al. (1982), applied this approach to helium and carbon infrared recombination lines observed in the spectrum of the WC8 star γ Vel and the method has since been applied to larger samples of WC stars (see below). In WO stars, the ionization conditions are extreme enough for such a recombination line abundance analysis to be further simplified; helium is all in the form of He^{2+}, carbon is all in the form of C^{4+}, and oxygen is

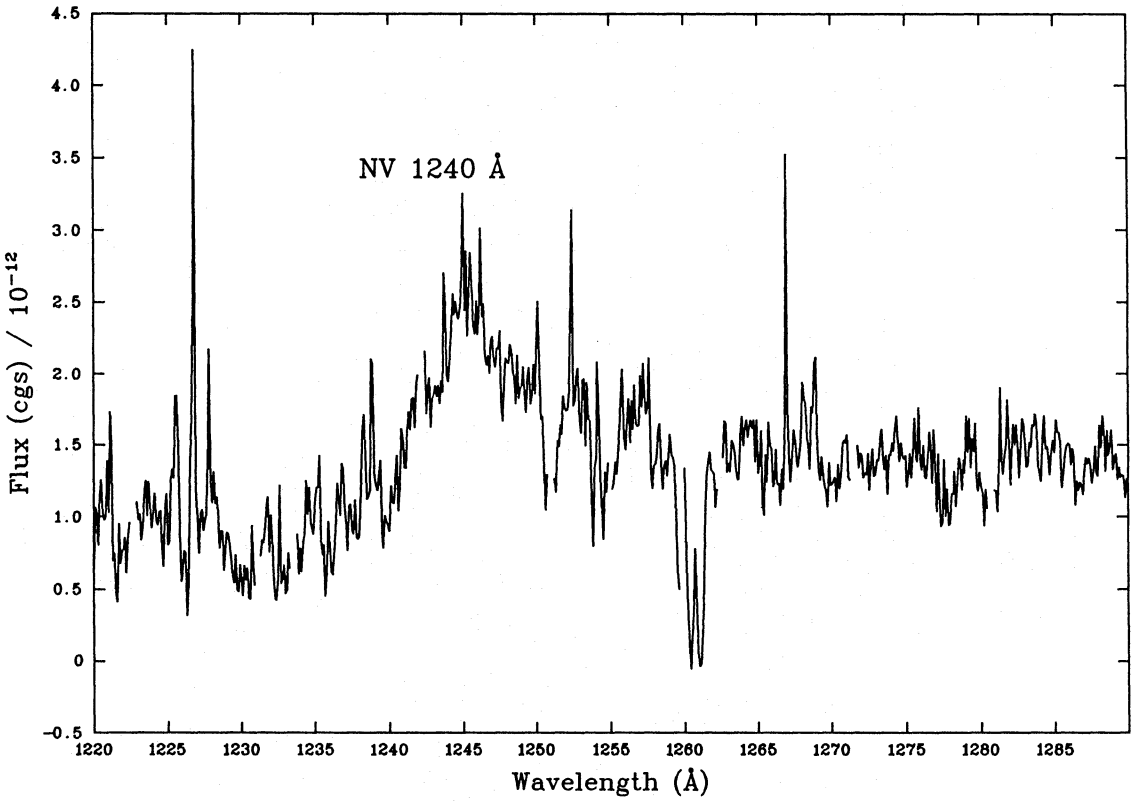

Fig. 5. A portion of the high resolution *IUE* spectrum of Sand 1 (SWP 7623). The feature identified is the N v 1238,1242 Å resonance doublet P Cygni profile, arising from the O7 primary

effectively all in the form of O^{4+}, O^{5+}, and O^{6+}. Lines of higher stages of ionization of oxygen are only weakly present in the spectrum of the WO1 star Sand 4, and can be shown (Sect. 8.3.3) to represent only trace stages of ionization in the winds of these stars. It is now well-known that the winds of Wolf–Rayet stars have considerable ionization stratification (e.g. Hillier 1989). However, Smith & Hummer (1988) have formally shown (in their Sect. 7.4) that even in a stratified wind the elemental abundances are exactly given by the sum of the individual ionic emission measures, provided that the inner radius down to which line and continuum opacity permits line emission to be observed is the same for each species. This is usually the case for recombination lines observed in a similar spectral region (e.g. in the optical), since the depth of recombination line formation is normally determined by a slowly-varying continuum opacity. Provided one pays careful attention to possible optical depth effects in the lines (especially for those between low-lying levels, or transitions whose upper levels are also connected to low lying levels) and chooses only lines which are optically thin in deriving abundances, recombination theory provides the most straightforward method for deriving abundances in WR star outflows. Carbon abundances in WC stars have been derived using recombination theory by Nugis (1982), Torres (1988), Smith & Hummer (1988) and Eenens & Williams (1992), while detailed non-LTE analyses of the WC5 star HD 165763 (WR 111) have been performed by Hillier (1989) and by Hamann et al. (1992). Torres analyzed the optical spectra of 74 WC stars using Case B recombination theory and derived C/He ratios between 0.13 and 0.79 by number. Her C^{3+} abundances were derived from the C III 5696 Å line, which Hillier (1989) warns could be partially thick. Torres found no significant trend of C/He ratio with WC subclass. Smith & Hummer (1988) analyzed infrared H and K band spectra of 15 WC stars and derived carbon abundances primarily using Case B recombination theory. Since there were no recombination coefficients available for the infrared recombination lines of C III, LTE was assumed in order to obtain lower limits on the C^{3+} abundance. As LTE abundances are underestimated by $\sim 1/b_n$, where b_n is the departure coefficient of the upper level, Smith and Hummer adopted b_n's derived for the C IV lines in order to estimate the extent of non-LTE effects in the C III lines. By multiplying the LTE C^{3+} abundances by ~ 10 $(1/b_n)$, they derived maximum C/He ratios of between 0.1 and 0.7. (The minimum C/He ratios derived by assuming LTE for C^{3+} were between 0.04 and 0.3.) Smith and Hummer claimed a trend of increasing C/He with earlier subclass, in contrast to the findings of Torres. The abundances that they derived were consistent with those of Torres for the stars in common. One WC4 star was included in the sample of Smith & Hummer, while ten were included in Torres' sample. Eenens & Williams (1992) analysed the IR spectra of six WC stars with higher resolution and increased spectral coverage compared to Smith & Hummer. They adopted a similar approach for the derivation of the C^{3+} abundances and also tentatively confirmed a trend of increasing C/He with earlier subclass (although no WC4 star

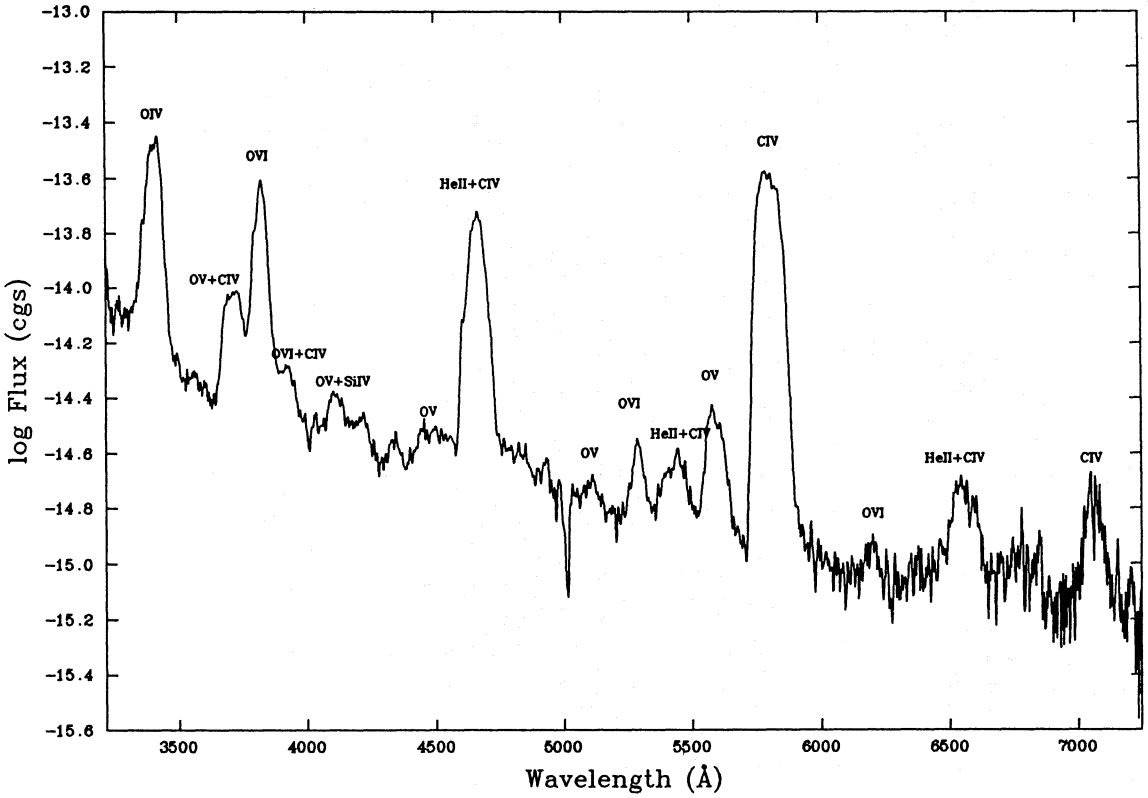

Fig. 6. The dereddened optical flux distribution of the WO4 star Sand 2, with the strongest emission features identified. The apparent absorption feature at 5000 Å is due to the subtraction of nebular [O III] $\lambda\lambda$4959,5007 emission in the off-star portion of the long-slit spectrum

was included in their survey). Their C/He values ranged from 0.07–0.41, consistent with those derived by Torres and by Smith & Hummer.

Hillier (1989) carried out a detailed non-LTE analysis of the WC5 stars HD 165763 (WR 111), and compared his model results to UV, optical and IR observations. His analysis was much more comprehensive in that it included excitation from the ground state and optical depth effects. A C/He number ratio of 0.5 was found to provide a reasonable fit to both the helium and carbon line strengths. Hamann et al. (1992) carried out a similar NLTE analysis of HD 165763 and also obtained satisfactory agreement with the observed line strengths and profiles for C/He = 0.5 by number. This value from the NLTE analyses agrees with the values derived for the same star by the recombination analyses noted above (C/He = 0.2: Nugis 1982; 0.4: Torres 1988; 0.18–0.51: Smith & Hummer 1988; 0.4: Eenens & Williams 1992), lending confidence to the abundances derived below from recombination theory for the WO stars.

8.2. A recombination analysis for the WO stars

We carried out a Case B optically thin recombination analysis (adopting T_e = 50 000 K and $n_e = 10^{11}$ cm^{-3} as characteristic values for the emitting regions), using the technique of Hummer et al. (1982). For a given ion i, the dereddened flux, I, in a recombination line is given by

$$I = \frac{Q}{4\pi D^2} \int_{V_i} n_i n_e \mathrm{d}V \tag{1}$$

where $Q = h\nu\alpha_{\rm eff}^{\rm rec}$, h is Planck's constant, ν is the frequency of the line, $\alpha_{\rm eff}^{\rm rec}$ is the effective recombination coefficient, D is the distance to the object and n_i and n_e are the local ionic and electron densities in the outflow. Integrating over the volume of emission,

$$I = \frac{Q}{4\pi D^2}[n_i] \, . \tag{2}$$

The ratio of the emission measures of two different ionic species can thus be obtained in a straightforward manner

$$\frac{[n_i]}{[n_j]} = \frac{I_i/Q_i}{I_j/Q_j} \tag{3}$$

To obtain the relative abundance for a pair of elements, one takes the ratio of the total emission measure for each of the elements, after summing over all observed ionization stages. Thus for elements X and Y, with number densities n(X) and n(Y),

$$\frac{n(\mathrm{X})}{n(\mathrm{Y})} = \frac{\sum_p [n(\mathrm{X}^{+p}]}{\sum_q [n(\mathrm{Y}^{+q}]} \tag{4}$$

The sources of the theoretical recombination line coefficients used here were as follows. For He II we used the tabulations of Hummer & Storey (1987) while for Li-like C IV and O VI we

made use of the results of Hummer & Storey (unpublished). For the remaining two ions of interest, O IV and O V, we have made new calculations of the recombination coefficients. We treat the ions as hydrogenic in the first instance, using the fully density dependent treatment of Hummer and Storey (1987). For transitions among relatively low-lying states we make allowance for radiative decays to non-hydrogenic states of the ground complex, using oscillator strengths from the Opacity Project (Cunto et al. 1993). Low temperature dielectronic recombination coefficients for O IV and O V lines were taken from the work of Nussbaumer & Storey (1984).

Our recombination analysis assumes that a) there is no self-absorption in the chosen lines, and b) that the recombination coefficients do not vary significantly with position in the wind. As demonstrated by Smith & Hummer (1988), the elemental abundance ratios given by the ratio of the sums of the emission measures of the individual ions of each element are completely independent of whether or not the ions are co-extensive with each other. One way of checking the validity of assumption (a) is to examine the internal consistency of the I/Q's derived from different transitions of a given ion. Disagreement between the I/Q's derived for the same ion could indicate that certain transitions of the ion are suffering from optical depth effects arising either from line self-absorption (for strong lines) or from continuum opacity (e.g. free-free absorption, which increases with wavelength in the infrared). Most emission features have more than one contributor present (e.g. all the He II $(n_1 - n_2)$ lines are blended with C IV $(2n_1 - 2n_2)$ transitions which occur at or near the same wavelength), so one must estimate the fractional contribution of each transition present. Lines which are free from blending (e.g. C IV 7062 Å) were used to predict the intensities of lines from the same ion in other blends, via recombination theory. The theoretical intensities for the C IV, O IV, O V and O VI lines were obtained by summing the Δl transitions predicted to fall within the observed wavelength range of a feature. The predicted contribution to a blend was subtracted from the total flux and the remaining flux was assigned to the other ionic contributor(s). To check the self-consistency of the final adopted intensities, the ratios of the final adopted C IV, He II and O VI intensities were compared to those predicted by recombination theory. Since the various contributors to a blend had their strengths predicted by normalization to unblended lines, agreement with recombination theory provides a good check on the self-consistency of this technique. The derived ratios for C IV, He II and O VI show satisfactory agreement with those predicted by recombination theory (Table 13). The satisfactory agreement found between the I/Q's derived from different transitions of a given ion validates the use of an optically thin recombination line analysis to derive abundances in the winds of these stars. These line fluxes were then used for the subsequent abundance analysis.

The Q's and derived I/Q's for the major transitions contributing to each emission feature are presented in Table 14. The final adopted I/Q for a given ion is based on a weighted mean of several lines in most cases; the weighting was based on the S/N of the feature and on the fractional contribution of the ion to the feature. Individual cases are discussed below.

8.3. Discussion of individual objects

8.3.1. Sand 1

He^{2+}: The adopted I/Q for He^{2+} was that given by the He II 1640 Å line alone, as He^{2+} was the dominant contributor to this feature. In the λ2511 and the λ4658+4686 blends, He^{2+} is only a minor contributor, hence the I/Q's from these transitions are more uncertain, but are nonetheless consistent with the adopted I/Q from λ1640. The S/N of the λ5411 feature is very poor and the relative contributions of He^{2+} and C^{4+} are extremely uncertain, so no weight was given to this line in the final I/Q adopted for He^{2+}

C^{4+}: The adopted I/Q for C^{4+} was given by a weighted mean from the transitions at λ2528 and λ4658+86. The highest weighting was given to 5–4 λ2528, as it is a strong transition and suffers from minimal blending (C IV + He II 2511 Å contributes $< 5\%$ to the flux in the observed feature). The full mechanism producing the doublet at 5801,12 Å is unknown; present NLTE models have difficulty reproducing its strength in WC5 stars, underestimating it by a factor of 3–5 (see Hillier 1989; Hamann et al. 1992). By contrast, from our current pure Case B recombination analysis of the WO stars, the I/Q derived from the λ5805 multiplet is usually *smaller* than derived from the other C IV lines (although by only 30–40% in the case of the two WO4 stars, versus factors of 2–4 for the WO2 and WO1 stars; see Table 14).

O^{4+}: The adopted I/Q for O^{4+} was based on the low temperature dielectronic recombination (LTDR) line at 1342 Å. High temperature dielectronic recombination processes (Burgess 1964) were considered to be unimportant at this high density. Due to its low-lying nature, its blending with other features and its susceptibility to other population mechansisms, O IV 3400 Å was not used to estimate the O^{4+} abundance for these stars.

O^{5+}: The O^{5+}+ abundance can in principle be derived from the 1371 Å LTDR line. However, the 1371 Å line is self-absorbed, showing a P Cygni profile (Fig. 4), which indicates a significant population in the lower level of this transition. A significant contribution to the emission component of the λ1371 feature may therefore arise from collisional excitation from the lower level, just as in the case of the C IV 1548,50 Å resonance feature in WC stars (Hillier 1989). In addition, the upper level of the O V λ1371 transition may be significantly populated by recombination of $1s^2$ 2p excited-state O VI (see Sect. 7), a process which is not accounted for by the radiative and low-temperature dielectronic recombination coefficients available to us. For these reasons, we have not used the O^{5+} I/Q obtained from the λ1371 line for our final abundance estimate. Other O V lines present in the spectrum of Sand 1 include the triplet 3p–3s and 3d–3p transitions, at 2786 Å and 5590 Å respectively. The 3d ^{3}D state can decay either to the 3p $^3P^0$, state or to 2p $^3P^0$. If the triplet 3d–2p

Table 13. Comparison between theoretical and dereddened line fluxes ratios for He II, C IV and O VI

ion	line ratio	theory	Sand 1	Sand 2	Sand 4	Sand 5
He^{2+}	1640/2511	45	45	39	–	–
	1640/4686	9.9	9.3	6.8	–	–
	1640/5411	107	288::	117	–	–
	2511/4686	0.22	0.21	0.18	–	–
	2511/5411	2.4	6.3::	3.0	–	–
	2511/6560	1.6	–	1.6	–	–
	4686/5411	11	30::	17	24:	9.9
	4686/6560	7.2	–	9.0	7.0	6.5
	5411/6560	0.70	–	0.52	0.30:	0.66
C^{4+}	1640/2511	30	30	18	–	–
	1640/2530	0.54	0.54	0.33	–	–
	1640/4658	1.6	1.6	0.93	–	–
	1640/5411	69	86	46	–	–
	2530/4658	3.0	3.0	2.2	–	–
	2530/5411	129	150	137	–	–
	2530/6560	70	–	77	–	–
	2530/7062	24	–	27	–	–
	4658/5411	43	51	49	54	41
	4658/6560	24	–	27	22	20
	4658/7062	8.0	–	9.6	7.9	7.7
	5411/6560	0.54	–	0.56	0.41	0.49
	5411/7062	0.19	–	0.19	0.15	0.19
	6560/7062	0.34	–	0.35	0.35	0.38
	7730/4658	0.45	–	–	0.30	0.33
	7730/5411	20	–	–	15	14
	7730/6560	11	–	–	6.2	6.7
	7730/7062	3.7	–	–	2.2	2.6
O^{6+}	5290/6200	3.5	–	6.0	4.6	3.7

Notes: theoretical Case B recombination line ratios are for $T_e = 5\times10^4$ K and $n_e = 10^{11}$ cm^{-3}.

λ192.9 transition were optically thin, the 3d ^{3}D state would decay to the 3p ^{3}P^0 state via the branching ratio 1/4029. However, at T_e = 50 000 K and $n_e = 10^{11}$ cm^{-3}, the 2p ^{3}P^0 state can acquire a significant population (up to 1/4 of the population of the ground state) and the triplet 3d–2p transition can become optically thick. Q(3d–3p) was derived assuming that all electrons in the 3d ^{3}D state decay to the 3p ^{3}P^0 level. Q(3p–3s) was derived assuming that the population of 3p ^{3}P^0 is the sum of direct recombinations to 3p and decays from 3d; all 3p electrons go to 3s. The I/Q derived from the λ5590 multiplet is lower than derived from the λ2786 multiplet in the case of both Sand 1 and Sand 2, which may indicate that the 3d ^{3}D – 2p ^{3}P^0 transition is not completely optically thick. We have therefore adopted as our final I/Q the value obtained from the λ2786 feature, since the I/Q derived from this multiplet is less susceptible to optical depth effects than that obtained from the λ5590 multiplet. The I/Q obtained from the very weak λ4930 7i–6h transition of O V is lower than that obtained from the λ2786 multiplet in the case of both Sand 1 and Sand 2. Since for each star the O^{5+} I/Q obtained from the λ4930 feature is less than the I/Q de-

rived for either O^{4+} or O^{6+}, we have chosen to retain the I/Q derived from the λ2786 multiplet. However, more work on the recombination theory and deeper spectra of these and further O V transitions is clearly desirable.

O^{6+}: The O^{6+} abundance for Sand 1 was based on the I/Q given by the 8–7 recombination line at 5290 Å. Other O VI lines are either weak or minor contributors to blends and were not used to derive I/Q's. The strong low-lying 3p–3s doublet at $\lambda\lambda$3811,34 is significantly stronger than predicted, relative to the 8–7 recombination line, which is similar to the behaviour of the analogous 3p–3s λ5801,12 doublet transition of C IV in the spectrum of the WC5 star HD 165763 (Hillier 1989; Hamann et al. 1992).

8.3.2. Sand 2

He^{2+}: The I/Q for He^{2+} is giyen by a weighted average of the I/Q's derived from the 1640 Å, 4686 Å and 6561 Å lines, where He^{2+} was a major contributor. The I/Q's from these lines show good agreement. The transitions at 2511 Å and 5411 A are weak and were not used for the final adopted I/Q for He^{2+}, although reasonable agreement is seen.

C^{4+}: The I/Q for C^{4+} was given by a weighted average from the 2528, 2907, 4658+86 and 5470 Å lines. As C IV 1640, 2511, 5411 and 6560 Å were not the major contributors to their blended features, their I/Q's were not included when deriving this average. The 9–7 λ7062 transition, a pure C IV feature, is in a region of the spectrum with somewhat poor S/N, leading to a large uncertainty in estimating the continuum level. Its derived I/Q is however within $\sim$ 5% of the overall adopted I/Q. The I/Q derived from C IV 5801,12 Å (Table 14) is a factor of 2.3 larger than the I/Q's derived from the other C IV lines.

O^{4+}, O^{5+}: The O^{4+} and O^{5+} I/Q's were derived in the same way as described above for Sand 1.

O^{4+}: The I/Q for O^{6+} was derived from λ5290 (8–7), as in the case of Sand 1. O VI 6200 Å (11–9, 13–11) is also present in our spectrum, but has rather poor S/N.

8.3.3. Sand 4

He^{2+}: Based on the apparent absence of He II lines from their optical and infrared spectra of Sand 4, Dopita et al. (1990) concluded that helium was absent and that Sand 4 reveals a naked C-O core. Here, on the other hand, we do find evidence for the presence of helium in our optical spectra of Sand 4, as did Polcaro et al. (1992). The published infrared spectrum of Dopita et al. (1990) covered a spectral region where no Δn = 1 He II transitions occur. The He II recombination lines falling within their spectral coverage included 7–5 at 1.16 μm, 10–6 at 1.28 μm and 11–6 at 1.17 μm, plus weaker transitions to the n = 8 and n = 9 levels. The strongest of these features, 7–5 at 1.16 μm, has the same upper level as He II 5411 Å, which we identify as a minor contributor to the λ5411, 5470 feature, so we would expect it to be weakly present. However, this line is blended in a strong feature with the O VI 3d–3p doublet at 1.18 μm and the C IV 8–7 transition at 1.19 μm. The strongest He II lines in the near-infrared are at 1.0124 μm and 1.8637 μm, the 5–4 and 6–5 transitions respectively, the latter occurring in a region where the Earth's atmosphere is opaque, while the former did not fall within Dopita et al.'s spectral coverage. UKIRT spectroscopy of Sand 4 has since shown that the He II 5–4 transition at 1.0124 μm is indeed present (Eenens 1993). In the optical region, the 4658+86 Å blend, and the 5411 Å and 6560 Å features all contain He II contributions. Transitions of C IV also contribute to these features, but the observed relative intensities (see Table 13) are consistent with the presence of He^{2+}.
The I/Q for He^{2+} was derived from the average of the I/Q's given by λ4686 and λ6560, emission features where He^{2+} was the major or a significant contributor. Due to the extremely large wind velocity of Sand 4, the $\lambda\lambda$5411, 5470 feature is partially blended with O V 5590 Å and O VI 5290 Å; its flux could be slightly underestimated.

C^{4+}: The I/Q adopted for C^{4+} was an average of the I/Q's derived from the features at 4658+86 Å, 6560 Å, 7062 Å and 1.73 μm. Eenens & Williams (1992) have demonstrated how the I/Q's derived for a given ion decrease with increasing infrared wavelength (their Fig. 1), due to the increase of free-free opacity with wavelength causing a reduction in the effective emitting volume observed (see also Sect. 8.4). For Sand 4 the C^{4+} I/Q's derived from the optical C IV lines are somewhat larger again than found from the 2.43 μm 10–9, 13–11 feature (Table 14). The 1.73 μm 9–8 transition however does have an I/Q within the range seen for the optical lines, and hence was included in the final average. We have not made use of lines longwards of $\sim$ 2μm when computing mean I/Q's. Smith & Hummer (1988) argued that the C^{4+}/He^{2+} ratio derived from the infrared recombination line spectra of WC stars really estimates $C^{4+}+O^{4+}/He^{2+}$, because the hydrogenic wavelengths of the infrared O IV transitions are the same as those of the corresponding C IV transitions, while O^{4+} would be expected to be the dominant stage of ionization of oxygen in the C^{4+} zone of WC stars. However, in the optical and ultraviolet spectral regions, O IV recombination lines do not have the same wavelengths as their C IV counterparts, so the C^{4+}/He^{2+} ratios derived from optical and ultraviolet recombination lines of C IV are indeed representative of carbon only. The WO1 and WO2 stars do not exhibit O IV lines in the optical, so no contribution from O IV to the infrared C IV lines is expected.

The C IV 7726+36 Å blend suffers from severe telluric absorption by the atmospheric A-band on the shortward side of the feature. Its total flux is consequently underestimated, leading to a derived I/Q which is about $\sim$ 40% lower than the adopted average.

C^{5+}: There is a broad feature between 4890 and 4995 Å in the spectrum of Sand 4, which we attribute to a blend of O V 7i-6h λ4930 and C V 7–6 λ4945. The dereddened flux in the feature is $1.44\,10^{-11}$ ergs cm^{-2} s^{-1}. If we adopt an O^{5+} I/Q of $1.46\,10^{13}$ cm^{-5}, from the O V 5590 Å, 1.55 μm and 2.10 μm lines (see below), and the Q-value in Table 14 for the 7i–6h

Table 14. I/Q's for strongest transitions and adopted I/Q for each ion

			Sand 1		Sand 2		Sand 4		Sand 5	
Ion	Transition	Q	I/Q	wt	I/Q	wt	I/Q	wt	I/Q	wt
He^{2+}	1640 (3–2)	2.36×10^{-24}	3.72×10^{12}	1	2.15×10^{12}	2	–		–	
	2511 (7–3)	5.21×10^{-26}	(3.70×10^{12})	0	(2.49×10^{12})	0	–		–	
	4686 (4–3)	2.38×10^{-25}	(3.94×10^{12})	0	(3.12×10^{12})	1	3.95×10^{14}	1	(2.09×10^{15})	1
	5411 (7–4)	2.20×10^{-26}	$(1.38\times10^{12}:)$	0	1.96×10^{12}	0	1.77×10^{14}	0	(2.29×10^{15})	0
	6561 (6–4)	3.28×10^{-26}	–	0	2.50×10^{12}	1	4.09×10^{14}	1	2.34×10^{15}	1
	Adopted		3.72×10^{12}		2.48×10^{12}		4.02×10^{14}		2.22×10^{15}	
C^{4+}	1640 (6–4)	1.06×10^{-24}	(3.01×10^{12})	0	(7.51×10^{11})	0	–		–	
	2511 (14–6)	3.56×10^{-26}	(3.01×10^{12})	0	(1.25×10^{12})	0	–		–	
	2530 (5–4)	1.98×10^{-24}	3.00×10^{12}	2	1.21×10^{12}	3	–		–	
	2907 (7–5)	4.15×10^{-25}	3.01×10^{12}:	0	1.41×10^{12}	1	–		–	
	4658+86 (6–5,8–6)	8.32×10^{-25}	3.02×10^{12}	1	1.32×10^{12}	2	1.95×10^{14}	2	1.12×10^{15}	2
	5411 (14–8)	1.53×10^{-26}	$(2.58\times10^{12}:)$	0	(1.14×10^{12})	0	(1.50×10^{14})	0	(1.16×10^{15})	0
	5470 (10–7)	6.06×10^{-26}	–		1.12×10^{12}	1	?		(1.22×10^{15})	0
	5801,12 (3p–3s)	1.39×10^{-24}	2.34×10^{12}	0	2.58×10^{12}	0	3.17×10^{13}	0	4.42×10^{14}	0
	6560 (12–8,7p–5s)	2.82×10^{-26}	–		(1.10×10^{12})	0	(2.00×10^{14})	1	(1.28×10^{15})	1
	7062 (9–7)	8.30×10^{-26}	–		1.08×10^{12}:	0	1.91×10^{14}	2	1.14×10^{15}	3
	7726+36 (7–6,11–8,14-9)	3.07×10^{-25}	–		–		1.15×10^{14}	0	7.91×10^{14}	0
	1.73μm (9–8)	5.43×10^{-26}	–		–		2.04×10^{14}	1	–	
	2.43μm (10–9,13–11)	3.52×10^{-26}	–		–		1.69×10^{14}	0	–	
	Adopted		3.01×10^{12}		1.26×10^{12}		1.96×10^{14}		1.16×10^{15}	
O^{4+}	1342 ($2p^3\ ^2D^0$–$2p^2\ ^2P$)	2.63×10^{-23}	4.18×10^{11}	1	8.79×10^{10}	1	–		–	
	3400 ($3d\ ^2D$–$3p\ ^2P^0$)	4.78×10^{-24}	1.77×10^{12}	0	6.69×10^{11}	0	–		–	
	Adopted		4.18×10^{11}		8.79×10^{10}		0		0	
O^{5+}	1371 ($2p^2\ ^1D$–$2s2p\ ^1P^0$)	3.37×10^{-23}	6.71×10^{11}	0	1.58×10^{11}	0	–		–	
	2786 (3p–3s)	1.24×10^{-23}	3.91×10^{11}	1	1.02×10^{11}	1	–		–	
	5590 (3d–3p)	4.33×10^{-24}	1.32×10^{11}	0	4.88×10^{10}	0	1.13×10^{13}	1	8.89×10^{13}	1
	4930 (7i–6h)	4.21×10^{-25}	1.64×10^{11}:	0	5.02×10^{10}::	0	–		–	
	1.55μm (10–9,13–11)	1.47×10^{-25}	–		–		1.97×10^{13}	1	–	
	2.10μm (11–10)	6.34×10^{-26}	–		–		1.29×10^{13}	1	–	
	Adopted		3.91×10^{11}		1.02×10^{11}		1.46×10^{13}		8.89×10^{13}	
O^{6+}	2080 (6–5,8–6,11–7)	8.52×10^{-24}	4.67×10^{11}	0	–		–		–	
	2915 (12–8)	2.21×10^{-25}	$(2.89\times10^{12}::)$	0	(1.61×10^{11})	0	–		–	
	3434+38 (7–6,11–8)	2.66×10^{-24}	–		–		5.86×10^{13}	0	1.90×10^{14}:	0
	3811,34 (3p–3s)	5.36×10^{-24}	9.88×10^{11}	0	3.60×10^{11}	0	3.17×10^{14}	0	9.90×10^{14}	0
	5290 (8–7)	1.05×10^{-24}	2.91×10^{11}	1	8.46×10^{10}	1	2.79×10^{13}	2	1.48×10^{14}	2
	6198+6200 (11–9,13–10)	3.06×10^{-25}	–		4.79×10^{10}:	0	2.08×10^{13}	1	1.37×10^{14}	1
	Adopted		2.91×10^{11}		8.46×10^{10}		2.55×10^{13}		1.44×10^{14}	

Notes to Table 14: Transitions which contribute < 50% of a given feature are in parentheses. Weightings are based on S/N of lines and relative contributions to features.

Table 15. WO abundances (by number)

	Sand 1	Sand 2	Sand 4	Sand 5
C^{4+}/He^{2+}	0.81	0.51	0.49	0.52
C^{5+}/He^{2+}	–	–	0.019	–
O^{4+}/He^{2+}	0.11	0.035	–	–
O^{5+}/He^{2+}	0.11	0.041	0.036	0.040
O^{6+}/He^{2+}	0.078	0.034	0.063	0.065
O^{7+}/He^{2+}	–	–	0.003	–
O^{8+}/He^{2+}	–	–	0.003	–
C/He	0.81	0.51	0.51	0.52
O/He	0.30	0.11	0.11	0.10
C/O	2.74	4.59	4.64	5.20
C+O/He	1.10	0.62	0.62	0.62

transition of O V, then 43% of the total flux in the feature is due to O V. For $T_e = 5\,10^4$ K and $n_e = 10^{11}$ cm^{-3}, the predicted Q for the 7–6 transition of C V is $1.09\,10^{-24}$ ergs cm^3 s^{-1}, so the implied I/Q for C^{5+} is $7.57\,10^{12}$ cm^{-5}. This corresponds to only 3.7% of the amount of carbon in the form of C^{4+} (Table 15).

O^{4+}: No lines of O IV are seen in the spectrum of Sand 4, or of Sand 5; these stars are presumably too hot for any of the oxygen to be in lower states than O^{5+}.

O^{5+}: Although the O V 5590 Å feature suffers from optical depth effects in the two WO4 stars (Sect. 8.3.1), yielding an I/Q a factor of ~ 3 lower than the adopted I/Q's for those two stars, here is better agreement seen with the I/Q derived from this line with the I/Q's derived from the near-IR features at 1.55 and 2.10 μm, in this higher excitation WO1 star. Thus the adopted I/Q for O^{5+} was the average of the I/Q's given by these three features. It is possible that the 2.10 μm line suffers from continuum absorption (as discussed in the case of C IV above), however as its I/Q was intermediate between the I/Q's of the other two features, it was included in the final average. The O^{5+} abundance for Sand 4 may possibly be underestimated, due to the aforementioned problems with the 5590 Å and 2.10 μm features.

O^{6+}: The I/Q for O^{6+} was derived using the 5290 Å and 6200 Å lines, both in reasonable agreement with each other. The I/Q given by (7–6,11–8) 3434 Å is also in reasonable agreement with the I/Q from the above two lines (Table 15). However, the λ3434 flux is uncertain due to the high reddening to Sand 4, and hence was not included in the final average.

O^{7+} and O^{8+}: As discussed in Sect. 7 a feature between 6025 and 6110 Å is due to a blend of O VIII 10–9, 13–11 $\lambda\lambda$6068, 6064 and O VII 12–10 6085 Å. The dereddened flux measured in the feature is $2.1\,10^{-12}$ ergs cm^{-2} s^{-1}, $\sim$ 1.5 times larger than measured by Polcaro et al. (1992; the fluxes measured for other lines in common show reasonable agreement). Making the assumption that there are comparable abundances of oxygen in the form of O^{7+} and O^{8+}, a Q of $3.02\,10^{-25}$ ergs cm^3 s^{-1} for O VII 12–10 and a Q of $1.72\,10^{-24}$ ergs cm^3 s^{-1} for O VIII 10–9 + 13–11 (all for $T_e = 5\,10^4$ K and $n_e = 10^{11}$ cm^{-3}) imply an I/Q of $1.0\,10^{12}$ cm^{-5} for each of O^{7+} and O^{8+}, with O VIII contributing 86% of the flux in the feature. Combined with the O^{5+} and O^{6+} abundances listed in Table 14 and 15, these values imply that, together, O^{7+} and O^{8+} contribute only 5.5% of the total oxygen abundance in the wind of Sand 4.

8.3.4. Sand 5

Ionic abundances for Sand 5 were derived in a similar manner as described above for Sand 4 and are listed in Table 14. No lines of C V or O IV were detected in the spectrum of Sand 5.

8.4. Total abundances

The weighted average I/Q's listed in Table 14 were used to derive total elemental abundance ratios. For all of the objects except the WO1 star Sand 4, C^{4+} is the only stage of ionization of carbon seen, and since the ionization potential to obtain C^{5+} is very high (392 eV), it is safe to assume that all carbon is in the form of C^{4+}. Even for the case of the highest excitation WO star, Sand 4, the fraction of carbon in the form of C^{5+} is only measured to be of the order of 3.7% (Sect. 8.3.3). Since He^{2+} is the only stage of ionization of helium seen, the C^{4+}/He^{2+} ratio gives the C/He ratio. Total oxygen abundances were derived by adding all the contributing ions (i.e. O/He = O^{4+}/He^{2+} + O^{5+}/He^{2+} + O^{6+}/He^{2+}). Elemental abundance ratios, by number, are presented in Table 15. Note the narrow range of the C/He and O/He ratios derived for these stars.

The likely accuracy of the abundances derived for each star can be gauged by the degree of agreement between the I/Q's derived from different lines of the same ion. The largest uncertainties in the adopted fluxes arise from the uncertainty in the adopted reddenings and the need to sometimes use lines located in low S/N regions of the spectra. Our abundance analysis of Sand 2, 4 and 5 assumed an intrinsic $F_\lambda \propto \lambda^{-3}$ flux distribution in the ultraviolet and optical for each star (see Sect. 5). This led, for each star, to C/He number ratios of 0.51 and O/He number ratios of 0.11. We also repeated the abundance analyses assuming an intrinsic $F_\lambda \propto \lambda^{-4}$ (i.e. Rayleigh-Jeans) flux distribution for each star. This yielded C/He number ratios of 0.41, 0.60 and 0.36 for Sand 2, 4 and 5, respectively, while O/He number ratios of 0.14, 0.15 and 0.083 were obtained for each star.

Errors in the assumed electron temperature and density should not greatly alter the final abundances. The weak temperature dependence of the recombination coefficients practically cancels out in the final abundance ratios. More serious could be the variation of the electron density over the emitting region for different ions. The recombination coefficients are a function of electron density, and the sensitivity to density depends on the ionic charge. Such effects would not therefore be expected to cancel out, as they tend to do for the temperature variations.

However, by repeating the analyses using recombination coefficients appropriate for electron densities a factor of ten higher and lower than those for $n_e = 10^{11}$ cm^{-3} adopted here, we find that such uncertainties should affect the derived ionic abundance ratios by less than 20%.

Variations in the continuum opacity can also affect the derived abundance ratios. The volume of emission of a line is determined by both the line opacity and the continuum opacity. The latter appears to be fairly constant in the optical/UV, where electron scattering is the dominant continuum opacity source, but in the infrared region free-free opacity, which increases as λ^2, becomes increasingly important. As a result, one sees less deep into the wind (i.e. a smaller volume is sampled) with longer wavelength infrared transitions. However, due to the short wavelength Wien turn-over, one only needs to correct for free-free opacity in the infrared. Hummer et al. (1982) in their analysis of the WC8 star γ Vel corrected their infrared line fluxes longward of 3 μm in order to compensate for this effect. Eenens & Williams (1992) found a trend of decreasing I/Q with increasing infrared wavelength when examining six WC stars, confirming that a smaller volume is indeed sampled at longer wavelengths. However, inspection of their Fig. 1 shows that this effect was minimal for lines shortward of 2.5 μm. The effect of free-free opacity can be directly seen in the infrared spectrum of Sand 5 presented by Eenens & Williams (1991), where the asymmetry in the line profiles increases with increasing wavelength; lines of longer wavelength are progressively more attenuated on the red side, due to the increasing continuum opacity with increasing wavelength. Here, as expected, we see no wavelength dependence for the I/Q's derived from lines in the UV and optical regions, confirming that corrections for continuum opacity are unnecessary for those regions. We do see a decrease in the I/Q's derived for Sand 4 from lines longwards of 2 μm (Sect. 8.3.3) and so the values obtained from these longer wavelength lines were not used for our final averages.

9. Discussion: carbon and oxygen abundances in WO stars

The C/He abundance ratios derived for the four WO stars (Table 15) exhibit a remarkably small range. Indeed, the C/H number ratios of Sand 2 (0.51), Sand 4 (0.51) and Sand 5 (0.52) are identical within the errors, despite the fact that the metallicity of the LMC host galaxy of Sand 2 is 2–3 times smaller than that of the Milky Way host galaxy of Sand 2. Sand 1, located in the SMC, whose metallicity is another fact of two lower than that of the LMC, does however have a larger C/He ratio, 0.81 by number. However, Sand 1 also has a larger O/He number ratio than the other three WO stars (see below), with the consequence that its carbon mass fraction of 0.52 is the same as those of the other WO stars (Table 16).

The C/He abundance ratios derived here for the WO stars are at the top end of the range of those derived for WC stars by Torres (1988), Smith & Hummer (1988), Eenens & Williams (1992) and Hillier (1989). When examining the C/He vs. subclass relation for WC stars, a general trend of higher C/He ratios for earlier type stars was proposed by Smith & Hummer, as well as by Eenens & Williams (1992), though there appears to be a spread in C/He values within any given subclass and the uncertainties affecting the derived C^{3+} abundances (see Sect. 8.1) particularly affect the middle and late-type WC stars. The C/He ratio for a given star should depend on the extent of nuclear processing in the progenitor star. The evolutionary stage at which a star enters and exits the WC stage is highly dependent on mass, metallicity and mass loss rate (Maeder 1991). Thus given the range of initial masses and initial abundances for stars that end up as WR stars, and given the uncertainties associated with the derived abundances, it is an open question whether a C/He ratio vs. subclass relation can alone be used to parameterize WC stars. Langer (1989) has argued that the stellar mass as well as the surface helium abundance are needed in order to completely describe all the observable properties of Wolf–Rayet stars.

Total oxygen abundances have not previously been derived for Population I WR stars. Only lower limits based on one or more stages of ionization have been derived, e.g. by Hillier (1989) and by Smith & Hummer (1988). Hillier (1989) estimated the C/O number ratio in the WC5 star HD 165763 to be greater than five, using the ratio of O^{3+} to C^{3+} abundances derived from fitting his model to observed O III and C III line fluxes. Smith & Hummer 1988) measured line fluxes for O V (10–9,13–11) at 1.55 μm and O VI (13–12) at 2.43 μm[3] for the WC4 and WC5 stars in their sample. Using LTE assumptions, they derived lower limits for the O^{5+} and O^{6+} abundances and compared them to the C^{4+} abundance, obtaining $C/O < 70$ for the WC4 star WR 19. With Q's derived from recombination theory, we derive $C/O < 13$ by number for this star using their line fluxes. This should provide a hard upper limit for the C/O ratio for this WC4 star, as oxygen should be predominantly in the O^{4+} and O^{3+} stages.

For the four WO stars analysed in detail here, we derive O/He number ratios of 0.11, 0.11 and 0.10 (i.e. identical within the errors) for Sand 2, 4 and 5, respectively, while their C/O number ratios show a narrow range between 4.6 and 5.2 (Table 15). As was also the case for its C/He ratio (see above), Sand 1, in the SMC, has a significantly higher O/He number ratio (0.30) than the other three WO stars, and its C/O number ratio of 2.7 is about a factor of two smaller than that found for the other three WO stars (Table 15).

Smith & Maeder (1991) and Maeder (1991) used the results of Smith & Hummer (1988) to parameterize the WC subclasses, based on their (C + O)/He ratios alone. Smith & Maeder proposed classifying WO stars as those having (C + O)/He > 1 by number. However, inspection of Table 15 reveals that only Sand 1 (a WO4 star), with (C + O)/He = 1.10, has (C + O)/He > 1. For the remaining three WO stars, (C + O)/He = 0.62.

Table 16 lists the derived helium, carbon and oxygen abundances by mass and compares them to those predicted by the solar metallicity evolutionary models of Schaller et al. (1992; essentially the same results were found by Maeder (1990) us-

[3] The flux in this feature was very uncertain, as it was just the remnant flux in a blend.

Table 16. WO abundances (by mass) and comparison to models of Schaller et al. (1992)

	X_{He}	X_C	X_O	initial Z
Sand 1 (WO4)	0.22	0.52	0.26	(0.003)
Sand 2 (WO4)	0.34	0.51	0.15	(0.007)
Sand 4 (WO1)	0.33	0.52	0.15	(0.02)
Sand 5 (WO2)	0.33	0.53	0.14	(0.02)
40 $M_\odot$ model, Z=0.02, stage 37	0.29	0.44	0.25	0.02
τ=4.6×10^6 yr, present M=13.2 $M_\odot$				
60 $M_\odot$ model, Z=0.02, stage 34	0.41	0.41	0.16	0.02
τ=3.7×10^6 yr, present M=18.8 $M_\odot$				
60 $M_\odot$ model, Z=0.02, stage 35	0.37	0.42	0.19	0.02
τ=3.7×10^6 yr, present M=16.1 $M_\odot$				
60 $M_\odot$ model, Z=0.02, stage 36	0.33	0.42	0.22	0.02
τ=3.7×10^6 yr, present M=14.0 $M_\odot$				
60 $M_\odot$ model, Z=0.02, stage 37	0.30	0.43	0.25	0.02
τ=3.7×10^6 yr, present M=12.5 $M_\odot$				

ing the older opacities). As can be seen, the range of oxygen mass fractions predicted for the various evolutionary stages of the models listed in Table 16 are all on the high side of the observed oxygen mass fractions. Moreover, the predicted carbon mass fractions at the relevant evolutionary stages (0.41–0.44) are systematically smaller than the carbon mass fraction of 0.52 derived here for each of the four WO stars. The Z = 0.02 evolutionary model surface abundances of Schaller et al. (1992) that best match those observed (Table 16) correspond to remnant stellar masses of 12–14 $M_\odot$. A 60 $M_\odot$ evolutionary model (60 WRA) of Woosley et al. (1993) predicted mass fractions similar to those found for the WO stars (Table 16) when the remnant stellar mass fell below 14 $M_\odot$.

Maeder (1990, 1991) calculated evolutionary models, using older opacities, for Z = 0.02, 0.005 and 0.002, and these models predicted a greater enhancement of the oxygen abundance at the WC/WO stage for lower initial metallicity stars. For Z = 0.02, Maeder (1990) predicted surface C/O number ratios ($\sim$ 2.5) similar to those derivable from Table 16 for the same stages of evolution of the Z = 0.02 models of Schaller et al. (1992), although a factor of two lower than the ratios of $\sim$ 5 derived here for the three Galactic and LMC WO stars (Table 15), i.e. these models predicted too much oxygen production. For Z = 0.005 however, Maeder (1990) only obtained WC/WO-type surface abundances for initial stellar masses of 85 $M_\odot$ and above, with such models predicting surface C/O number ratios of about unity during the relevant evolutionary stages, compared to the C/O number ratios of 2.7 found for Sand 1 (SMC metallicity $Z \sim 0.003$) and 4.6 found for Sand 2 (LMC metallicity $Z \sim 0.007$), i.e. the models again predicted too much oxygen production. Schaller et al. (1992) computed evolutionary models for an initial metallicity of Z = 0.001, but such low-metallicity models were not found to produce WC/WO stars for any initial mass.

Meynet et al. (1994) have calculated massive star evolutionary models which differed from those of Schaller et al. (1992) in adopting mass loss rates enhanced by a factor of two during the main sequence phase and, in some cases, during the WNL post-main sequence phase too. A comparison between our derived abundances and those predicted by the models of Meynet et al. is presented in Table 17. The Meynet et al. Z = 0.02 and 0.008 models are now able to reproduce the oxygen mass fractions of 0.15 derived for Sand 2, 4 and 5, but still predict too little carbon, typically X(C) = 0.44, compared to the values of X(C) = 0.52 observed, while predicting too much helium, typically X(He) = 0.40, compared to the values of X(He) = 0.33 that are observed. Stage 40 of the 120 $M_\odot$ Z = 0.02 model of Meynet et al. gets closest to the observed mass fractions of Sand 2, 4 and 5. One further success of the Meynet at al. (1994) models is that they predict that the He, C and O mass fractions of Galactic WO stars should not differ greatly from those of LMC WO stars (see their Z = 0.02 and Z = 0.008 models listed in Table 17), in accord with our observations of Sand 2, 4 and 5. In addition, the Meynet et al. models produced oxygen mass fractions during the WO phase of their Z = 0.003 models that were nearly double those during the WO phases of their higher metallicity models (see Table 17), again in accord with our observations: we find that Sand 1, in the SMC, has an oxygen mass fraction of 0.26, versus the oxygen mass fractions of 0.15 derived for Sand 2, 4 and 5. As we also noted above in the context of their higher metallicity models, the Meynet et al. Z = 0.003 models predict helium mass fractions that are a little too high,

Table 17. WO abundances by mass and comparison to models of Meynet et al. (1994)

X(He)	X(C)	X(O)	Z	
0.33	**0.53**	**0.14**	**0.02**	**Sand 5**
0.36	0.46	0.15	0.02	stage 39, 40$M_\odot$, $\dot{M}$ x2 in MS, WNL
0.42	0.42	0.13		stage 34, 40$M_\odot$, $\dot{M}$ x2 in post-MS
0.38	0.43	0.15		stage 35, 40$M_\odot$, $\dot{M}$ x2 in post-MS
0.41	0.41	0.16		stage 34, 60$M_\odot$, reg. $\dot{M}$
0.40	0.43	0.14		stage 36, 60$M_\odot$, $\dot{M}$ x2 in MS, WNL
0.39	0.44	0.14		stage 37, 60$M_\odot$, $\dot{M}$ x2 in post-MS
0.36	0.45	0.16		stage 38, 60$M_\odot$, $\dot{M}$ x2 in post-MS
0.40	0.44	0.13		stage 38, 85$M_\odot$, $\dot{M}$ x2 in MS, WNL
0.37	0.44	0.15		stage 39, 85$M_\odot$, $\dot{M}$ x2 in MS, WNL
0.40	0.41	0.16		stage 35, 85$M_\odot$, $\dot{M}$ x2 in post-MS
0.35	0.47	0.15		stage 40, 120$M_\odot$, $\dot{M}$ x2 in post-MS
0.33	**0.52**	**0.15**	**0.02**	**Sand 4**
0.29	0.44	0.25	0.02	stage 37, 40$M_\odot$, reg. $\dot{M}$
0.32	0.47	0.18		stage 40, 40$M_\odot$, $\dot{M}$ x2 in MS, WNL
0.37	0.42	0.19		stage 35, 60$M_\odot$, reg. $\dot{M}$
0.37	0.44	0.16		stage 37, 60$M_\odot$, $\dot{M}$ x2 in MS, WNL
0.39	0.44	0.14		stage 37, 60$M_\odot$, $\dot{M}$ x2 in post-MS
0.31	0.47	0.19		stage 41, 85$M_\odot$, $\dot{M}$ x2 in MS, WNL
0.30	0.49	0.18		stage 43, 120$M_\odot$, $\dot{M}$ x2 in post-MS
0.34	**0.51**	**0.15**	**0.007**	**Sand 2**
0.41	0.44	0.14	0.008	stage 36, 60$M_\odot$, $\dot{M}$ x2 in MS, WNL
0.37	0.45	0.16		stage 37, 60$M_\odot$, $\dot{M}$ x2 in MS, WNL
0.42	0.43	0.15		stage 35, 85$M_\odot$, $\dot{M}$ x2 in MS, WNL
0.43	0.43	0.13		stage 38, 120$M_\odot$, $\dot{M}$ x2 in MS, WNL
0.22	**0.52**	**0.26**	**0.003**	**Sand 1**
0.26	0.44	0.29	0.004	stage 38, 60$M_\odot$, $\dot{M}$ x2 in MS, WNL
0.28	0.42	0.29		stage 37, 85$M_\odot$, $\dot{M}$ x2 in MS, WNL
0.27	0.44	0.28		stage 38, 120$M_\odot$, $\dot{M}$ x2 in MS, WNL

and carbon mass fractions that are a little too low, compared to those derived for Sand 1.

Acknowledgements. We thank Dr. J.R. Deacon for convolving our optical spectrophotometry of Sand 5 with theoretical UBV filter profiles in order to predict the equivalent magnitudes. We are also grateful to Dr. P.A. Crowther for calculating several WC/WO star models in order to check the theoretical continuum energy distributions.

References

Barlow J., 1987, MNRAS 227, 161
Barlow M.J., Blades J.C., Hummer D.G., 1980, ApJ 241, L27
Barlow M.J., Hummer D.G., 1982, in: de Loore C.W.H., Willis A.J. (eds.) IAU Symp. No. 99, Wolf-Ravet Stars, Observations, Physics, Evolution. Reidel, Dordrecht, p. 387
Beals C.S., Plaskett H.H., 1935, in: Trans. IAU 5, Report on the Sub-Committee of Commission 29 on the Classification of WR Stars, p. 184
Bohlin R.C., Grillmar C.J., 1988, ApJS 66, 209
Burgess A., 1964, ApJ 139, 776
Burstein D., Heiles C., 1982, AJ 87, 1165
Clavel J., Gilmozzi R., Preito A., 1986, IUE ESA Newsletter 26, p. 65
Cohen M., Walker R.G., Barlow M.J., Deacon J.R., 1992, AJ 104, 1650
Conti P.S., Alschuler W.R., 1971, ApJ 170, 325
Cunto W., Mendoza C., Ochsenbein F., Zeippen C.J., 1993, A&AS 275, L5
Davidson K., Kinman T.D., 1982, PASP 94, 634
Dopita M.A., Lozinskaya T.A., McGregor P.J., Rawlings S.J., 1990, ApJ 351, 563
D'Odorico S., Rosa M., 1982, A&A 105, 410
Eenens P.R.J., 1993, in: Cassinelli J.P., Churchwell E.B. (eds.) ASP Conf. Series Vol. 35, Massive Stars, Their lives in the ISM, p. 254
Eenens P.R.J., Williams P.M., 1991, in: Jaschek C., Andrillat Y. (eds.) Proc. Montpellier Conf., The IR Spectral Region of Stars, p. 158
Eenens P.R.J., Williams P.M., 1992, MNRAS 255, 227
Esteban C., Smith L.J., Vilchez J.M., Clegg R.E.S.C., 1993, A&A 272, 299
Fitzpatrick E.L., 1985, ApJS 59, 77
Garnett D.R., Kennicutt R.C., Chu Y., Skillman E.D., 1991, ApJ 373, 458
Hamann W.-R., Leuenhagen U., Koesterke L., 1992, A&A 255, 200
Hillier D.J., 1989, ApJ 347, 392
Hindman J.V., 1967, Aust J Phys 20, 147
Howarth I.D., 1983, MNRAS 203, 301
Howarth I.D., Murray J., 1988 SERC STARLINK User Note No. 50
Howarth I.D., Prinja R.K., 1989, ApJ 69, 527
Howarth I.D., Schmutz W., 1992, A&A 261, 503
van der Hucht K.A., Conti P.S., Lundstrom I., Stenholm B., 1981, Space Sci. Rev. 28, 227
Hummer D.G., Storey P.J., 1987, MNRAS 224, 801
Hummer D.G., Barlow M.J., Storey P.J., 1982, in: de Loore C.W.H., Willis A.J. (eds.) IAU Symp. No. 99, Wolf–Rayet Stars, Observations, Physics, Evolution. Reidel, Dordrecht, p. 79
Kingsburgh R.L., Barlow M.J., 1995, A&A (in press)
Koornneef J., 1982, A&A 107, 247
Kurucz R.L., 1991, in: Davis Philip A.G., Upgren A.R., Lanes K.A. (eds.) proceedings of the workshop on "Precision Photometry, Astrophysics of the Galaxy". L. Davis Press, Schenectady, p. 27
Lake G., Skillman E.D., 1988, AJ 98, 1274
Lamla E., 1982, in: Schaifers K., Voigt H.H. (eds.) Landolt-Börnstein, Numerical Data and Functional Relationships in Science and Technology, Group VI, Astronomy, Astrophysics and Space Research, Vol. 2b. Berlin
Langer N., 1989, A&A 210, 93
Maeder A., 1990, A&AS 845, 139
Maeder A., 1991, A&A 242, 93
Meynet G., Maeder A., Schaller G., Schaerer D., Charbonel C., 1994, A&AS 103, 97
Moffat A.F.J, Seggewiss W., 1984, A&AS 58, 117
Moffat A.F.J., Breysacher J., Seggewiss W., 1985, ApJ 292, 511
Moffat A.F.J., Niemela V.S., Seggewiss W., Magalhaes A.M., Cerruti M.A., 1991, in: van der Hucht K.A., Hidayat B. (eds.) IAU Symp. No. 143, Wolf–Rayet Stars and Interrelations with Other Massive Stars in Galaxies, Kluwer, Dordrecht,p. 257
Morris P.W., Brownsberger K.R., Conti P.S., Massey P., Vacca W.D., 1993, ApJ 412, 324
Nugis T., 1982, in: de Loore C.W.H., Willis A.J. (eds.) IAU Symp. No. 99, Wolf–Rayet Stars, Observations, Physics, Evolution. Reidel, Dordrecht, p. 131
Nussbaumer H., Storey P.J., 1984, A&AS 56, 293
Oke J.B., 1974, ApJS 27, 21
Polcaro V.F., Viotti R., Rossi C., Norci L., 1992, A&A 256, 563
Prevot M.L., Lequeux J., Prevot L., Maurice E., Volmerange P., 1984, A&A 132, 389
Prinja R.K., Barlow M.J., Howarth I.D., 1990, ApJ 361, 607
Reid I.N., Strugnell P.R., 1986, MNRAS 221, 887
Rohlfs K., Kreitschmann J., Seigman B.C., Feitzinger J.V., 1984, A&A 137, 343
Rustamov D.N., Cherepaschuk A.M., 1987, Soviet Astron. Lett. 13, 286
Saha A., Freedman W.L., Hoessel J.G., Mossman A.E., 1992, AJ 1045, 1072
Sandage A.R., 1971, ApJ 166, 13
Sanduleak N., 1971, ApJ 164, L71
Schaller G., Schaerer D., Meynet G., Maeder A., 1992, A&AS 96, 269
Schmutz W., Leitherer C., Gruenwald R., 1992, PASP 104, 1164
Seaton M.J., 1979, MNRAS 187, 73
Shortridge K., 1989, SERC STARLINK User Note No. 86
Smith L.F., 1968, MNRAS 138, 109
Smith L.F., Hummer D.G., 1988, MNRAS 230, 511
Smith L.F., Maeder A., 1991, A&A 241, 77
Smith L.F., Shara M.M., Moffat A.F.J., 1990a, ApJ 348, 471
Smith L.F., Shara M.M., Moffat A.F.J., 1990b, ApJ 358, 229
Straede J., 1980, AAO Preprint No. 135
Talavera A., 1988, ESA IUE Newsletter 30
Torres A.V., 1988, ApJ 325, 759
Turner D.G., 1982, in: de Loore C.W.H., Willis A.J. (eds.) IAU Symp. No. 99, Wolf–Rayet Stars, Observations, Physics, Evolution. Reidel, Dordrecht, p. 57
Turner D.G., Forbes D., 1982, PASP 91, 789
Wessolowski U., Schmutz W., Hamann, W-R., 1988, A&A 194, 160
Willis A.J., Schild H., Smith L.J., 1992, A&A 261, 419
Woosley S.E., Langer N., Weaver T.A., 1993, ApJ 411, 823